Feedback mechanism in the oceanic carbon cycle

by

Takamitsu Ito

Submitted to the Department of Earth Atmospheric and Planetary Sciences
in partial fulfillment of the requirements for the degree of

Master of Science in Geosystems

at the

MASSACHUSETTS INSTITUTE OF TECHNOLOGY

May 1999

Author .....
Department of Earth Atmospheric and Planetary Sciences
May 7, 1999

Certified by .....
Jochem Marotzke
Associate Professor
Thesis Supervisor

Accepted by .....
Ronald G. Prinn
Chairman, Department of Earth Atmospheric and Planetary Sciences

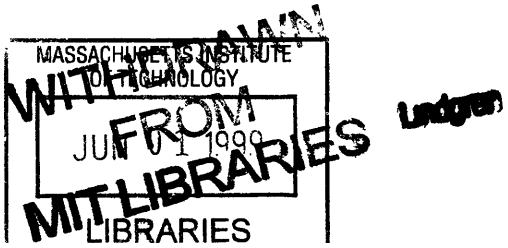

Feedback mechanism in the oceanic carbon cycle

by

Takamitsu Ito

Submitted to the Department of Earth Atmospheric and Planetary Sciences
on May 7, 1999, in partial fulfillment of the
requirements for the degree of
Master of Science in Geosystems

Abstract

In this thesis, I designed and implemented a simple atmosphere-ocean coupled carbon cycle model which can be used as a tool to uncover the mechanisms of the interaction between the dymanics of the atmosphere-ocean system and the oceanic reservior of CO_2 on the 10^1 to 10^3 years time scale. The atmosphere-ocean coupled model is originally developed by Marotzke (20,21), and the biogeochemical model is developed by Follows(personal communication). The atmosphere-ocean-carbon model makes the atmophere-ocean dynamics and the carbon cycle fully interactive, and results in two stationary states characterized by two distinct patterns of the thermohaline circulation. The temperature driven, high latitudes sinking mode showed significantly lower atmospheric pCO_2 than the salinity-driven, low latitudes sinking mode. The atmosphere-ocean dynamics dominates the system behavior of the model. The carbon cycle weakly feedbacks on the atmosphere-ocean system through the radiation balance. The model reveals two feedback mechanisms, the global warming feedback and the thermohaline pCO_2 feedback. The thermohaline pCO_2 feedback has three sub-components, which are the biological pump feedback, the outgassing feedback and the DIC exporting feedback. The numerical experiments estimate the relative importance among them. The system becomes less stable when all the feedback mechanism is introduced. The model could be used to understand some basic mechanism of the situations similar to the anthropogenic global warming. The stability analysis is applied to evaluate the model runs. The current rate of 7 GTC yr^{-1} can induce the spontaneous shutdown of thermohaline circulaiton after 550 years of constant emission. The stability of the thermohaline circulation rapidly decreases even before the system stops the thermohaline circulation. The model parameterized surface alkalinity as a simple function of sea surface salinity or as a constant, rather than solving the alkalinity cycle explicitly. The system is sensitive to the parameterization, in which different assumptions on alkalinity lead to different results both analytically and numerically.

Thesis Supervisor: Jochem Marotzke
Title: Associate Professor

Acknowledgments

I thank my family and friends both in Japan and in United States for encouragement and support. I thank professor J. Marotzke and M. Follows for instruction. I thank 1998-1999 Geosystems classmates.

Contents

List of Figures

List of Tables

Chapter 1

Introduction

Empirical and theoretical studies conducted since the 1980's have established a clear, but incompletely understood, relationship between climate and deep-ocean circulation. Geological data reveals that the pattern of deep-water circulation abruptly changed in the last glacial-interglacial period (6). Numerical experiments have also shown that a rapid increase in atmospheric carbon dioxide can weaken or halt the thermohaline circulation in the Atlantic ocean (18,28). Moreover, recent research suggests that the halt of thermohaline circulation could cause a considerable reduction of carbon dioxide uptake into the ocean (25).

These works suggest that a change in ocean circulation can have a significant effect on the distribution of carbon in the ocean and atmosphere. They also imply that there could be a feedback mechanism between the stability of thermohaline circulation and the greenhouse effect. In the last few decades, increasing concern about global warming resulting from further fossil fuel emissions have encouraged observational and modeling research to understand and quantify the mechanisms of the global carbon cycle. However, the relationship between the dynamics of atmosphere-ocean coupled system and the global carbon cycle is not well understood.

In this study, I construct a simple atmosphere-ocean coupled box model, combine it with an appropriate box model for the global carbon cycle, and use the result as a tool for understanding the mechanism of interaction between the dynamics of the coupled system and the oceanic reservoir of carbon dioxide. This study aims to

uncover feedback processes which can affect the circulation of the atmosphere and the ocean and the distribution of carbon in the ocean. The atmosphere-ocean coupled part of the model is similar to the coupled box model by Marotzke (20,21). The model is rich in its dynamic behavior where the intensity and the direction of the thermohaline circulation is controlled by the temperature and the salinity differences between high and low latitude oceans. The carbon cycle part was originally developed by Follows(personal communication) and is somewhat similar to the 3 box carbon cycle model by Toggeweiler and Sarmiento (24). This model represents the simplified biogeochemical cycle of carbon dioxide and carbonate species in the ocean.

This study newly introduces a simplified parameterization for the temperature and salinity dependencies of the carbon chemistry, which makes it possible to couple the atmosphere-ocean system with the carbon system. This study also modifies the atmosphere-ocean model by Marotzke so that the model has an idealized representation for the deep ocean. Although the model only covers the oceanic carbon cycle and the effect of the terrestrial biosphere is neglected, it is sensible to look at the oceanic carbon cycle for understanding the effect of the dynamics of the atmosphere-ocean coupled system.

Box models approximate complicated systems with simplified interactions of several boxes. The model has to be simple enough to be tractable, but must also be complicated enough to illustrate some of fundamental complexity of the system. Using the model, I investigated how the dynamics of the atmosphere and the ocean, such as the effect of transport of moisture and heat in the atmosphere or physical circulation of the ocean, interacts with the partial pressure of CO_2 in the atmosphere (pCO_2). Due to its simplicity, the model turns out to be an effective tool for exploring the global carbon cycle in a coupled atmosphere-ocean system.

Chapter two describes the architecture of the model and how the two parts (the atmosphere-ocean coupled model and the global carbon cycle model) of the model are coupled.

Chapter three describes the stationary states of the numerical model and discusses what determines the capacity of the ocean as a reservoir of CO_2.

Chapter four first discusses the feedback mechanisms and the stability of the system. Later sections shows some model runs under a similar condition to the anthropogenic global warming. This study is not intended to give a realistic simulation of the global warming but it suggests possible mechanisms of fundamental interactions involved in the global warming.

1.1 Climate variation and atmospheric CO_2

We know that there were some periods in Earth's history when the climate was quite different from that of today. One of the reasons could be that the ocean behaved very differently from that of today and contributed to different patterns of transport and distribution of heat and moisture. Geological studies conducted since the 1980's have surveyed the relationship between climate and deep-ocean circulation. Isotopic data suggests that the pattern of deep-water circulation abruptly changed in the last glacial-interglacial period (6). The Oxygen isotopic ratio, which is referred to $\delta^{18}O$, reflects the temperature of the air over the ice cap. The more negative the $\delta^{18}O$ value, the colder the air temperature. The age of the ice was determined by the depth of the ice core. $\delta^{18}O$ records from Greenland ice cores revealed climate oscillations in the Northern Atlantic during the last 100,000 years. Figure 1-1 shows oxygen isotope records of ice cores from Byrd, Antarctica (left) and Century, Greenland (right). The last glacial period ends around 12,000 to 11,000 years ago according to the isotopic record.

Ice core records also reveal that the time variation of pCO_2 and oxygen isotopic ratio are strongly correlated with each other. In Figure 1-2, the oxygen isotopic ratio is compared with pCO_2 trapped by Antarctica ice cores (23). The concentration of atmospheric CO_2 and the temperature of the air over the polar cap are strongly coupled. CO_2 is one of the well-known greenhouse gases, which traps the Earth's infrared radiation and keeps the surface of the planet warm. The strong coupling of pCO_2 and oxygen isotopic ratio implies that atmospheric CO_2 has a significant relationship with climate changes.

The CO_2 concentration in the atmosphere is about 360 parts per million by volume (ppmv) today, and is increasing about 1.5 ppmv each year. The CO_2 concentration in the atmosphere has been accurately monitored for approximately 40 years until now, and it has been rising at a rate of only 60% of the rate expected if all the fossil fuel released remained in the atmosphere (7). The fate of the remaining CO_2 is not precisely known because of the large uncertainty in terrestrial and oceanic uptake of CO_2. Figure 1-3 is a schematic diagram for the estimation of the carbon budget on the surface of Earth. The ocean is by far the largest reservoir of carbon and contains one of the most uncertain distributions of natural and anthropogenically released carbon. Therefore, perturbations in the ocean circulation could have a significant impact on the global carbon distribution.

Much experimental and modeling research has been aiming at describing the mechanisms of the oceanic carbon cycle and quantifying what will happen in the future with further fossil fuel emissions and potential perturbations to the carbon cycle through climate changes (14,26,27,28,29). The atmosphere-ocean-carbon climate system is quite complicated, which involves various subsystems such as atmosphere-ocean system, biogeochemical cycles, and hydrological cycles (27). There is a limitation in the quality and quantity of observasional data and climatic records. Numerical simulation is limited by the computational power, the chaotic behavior of the system, and unresolved subprocesses. Therefore, a simple model could be useful tool to understand the basic mechanism and the first-order approximate behavior of the complicated system. Comparing complicated models with simple models could enhance the understanding of the large scale behavior of the system, and simple models can isolate each interaction and evaluate the relative importance of indivisual mechanisms.

1.2 Interaction between the thermohaline circulation and the oceanic carbon cycle

Numerical experiments suggest that a rapid increase in atmospheric carbon dioxide can weaken or halt the thermohaline circulation in the Atlantic Ocean (18,28). Thermohaline circulation is driven by temperature and salinity differences between low and high latitudes. It plays a critical role in the transport of heat in the ocean (13). Salinity plays a crucial role in the thermohaline circulation in the Atlantic Ocean. Saline water is brought by the surface current from low latitudes, where the evaporation of surface water forms warm and saline water. North Atlantic Deep Water (NADW) sinks because the water is sufficiently dense due to cold temperature and relatively higher salinity (8). Since the late 1980s, several experiments have found that the rapid CO_2 growth in the atmosphere will cause a rise in global mean temperature, resulting in vigorous evaporation at low latitudes and precipitation at high latitudes. The increased moisture transport can cause lower salinity in the Northern Atlantic, and it can eventually weaken or stop the thermohaline circulation. Figure 1-4 is the temporal variation of the intensity of the thermohaline circulation in the North Atlantic in the general circulation model (GCM) result of Manabe and Stouffer (18). Gradually doubled atmospheric CO_2 temporarily slows down the formation of NADW by half, and quadrupled CO_2 permanently stops it.

Sarmiento and Quere (25) argued that the collapse of thermohaline circulation, in turn, can cause considerable reduction of carbon dioxide uptake by the ocean. Their three-dimensional GCM simulation revealed that the weakened thermohaline circulation could reduce the supply of nutrients in the southern ocean because of the weakened vertical mixing. The depletion of nutrients considerably reduces CO_2 uptake by stopping photosynthesis. The increase of sea surface temperature (SST) also decreases the solubility of CO_2 in the ocean. Although the sensitivity of the oceanic ecosystem is not well understood yet, their work suggests that a change in ocean circulation can possibly have a significant effect on the global carbon cycle.

The response of the oceanic carbon cycle to global warming was recently simu-

lated using an atmosphere-ocean coupled GCM for the period 1765 - 2065 (26). The model increases pCO_2 based on the observation until 1990 and the prediction by the International Panel of Climate Change (IPCC). Stouffer, Sarmiento, and others found the weakened thermohaline circulation and the large fluctuation of CO_2 uptake in the Southern Ocean. The solubility pump became very inefficient because of the increased SST, whereas the biological pump seemed to be activated. These results included an uncertainty that depends on different assumptions on the controlling parameter of the biological pump, but it is clear that a change in heat and moisture transport in the ocean could have a considerable impact on the oceanic CO_2 uptake. One of the essential findings of the numerical studies discussed above is that weakening thermohaline circulation and stratification of the mixed layer can perturb advective transport of carbon and nutrients in the ocean. It can also affect the oceanic CO_2 uptake through perturbing both the biological and the solubility pumps. There could be some feedback mechanism that relates the efficiency of the solubility and the biological pumps to the stability of thermohaline circulation. One of the goals of this study is to identify the response of the solubility and the biological pumps to the perturbation of atmosphere-ocean coupled system.

1.3 The atmosphere-ocean-carbon (AOC) box model

In chapter 3, I will present possible mechanisms of the interaction between the atmosphere-ocean coupled system and the global carbon cycle. The efficiency of the biological and the solubility pump is closely related to SST, salinity (SSS), and the intensity of the thermohaline circulation. pCO_2, in turn, influences the radiation balance of the atmosphere and the ocean, which determines SST, SSS, and the thermohaline intensity. A similar coupled climate-carbon box model was previously studied by Helen Johnson (personal communication), which was the first attempt to understand the interaction between the thermohaline circulation and the carbon cycle using an idealized model. Joos et al (15) recently showed a feedback mechanism in a global warming simulation using a 2-dimensional physical-biogeochemical climate

model, which focused on the global warming simulation. This study introduces a fully interactive atmosphere-ocean-carbon (AOC) box model, which aims to elucidate several fundamental feedback mechanisms between the atmosphere-ocean (AO) system and the carbon cycle (C) system. The AOC model is a combination of two models which are the atmosphere-ocean (AO) model (20,21) and the global carbon cycle (C) model (Follows : personal communication). The fully coupled AOC model simulates the AO and the C model jointly, including the radiation balance, precipitation, ocean circulation, biological activity, and the carbon chemistry in the sea water. The fully coupled model has fewer prescribed parameters than the uncoupled AO or C model. The AOC model inherits the explicit representation of the thermohaline intensity from the AO model, which is particularly useful to describe various feedbacks involving the thermohaline circulation (20,21). The C model provides a Newtonian damping formulation for the global carbon cycle with a characteristic time scale. Moreover, a simplified expression for the carbon chemistry makes it possible for the C model to calculate the effect of SST and SSS on the solubility pump in a very transparent way. In the following chapter, the structure of the uncoupled AO model, the C model, and the fully coupled AOC model are described in detail.

Figure 1-1: Broecker et al. (1985) : Oxygen isotope records

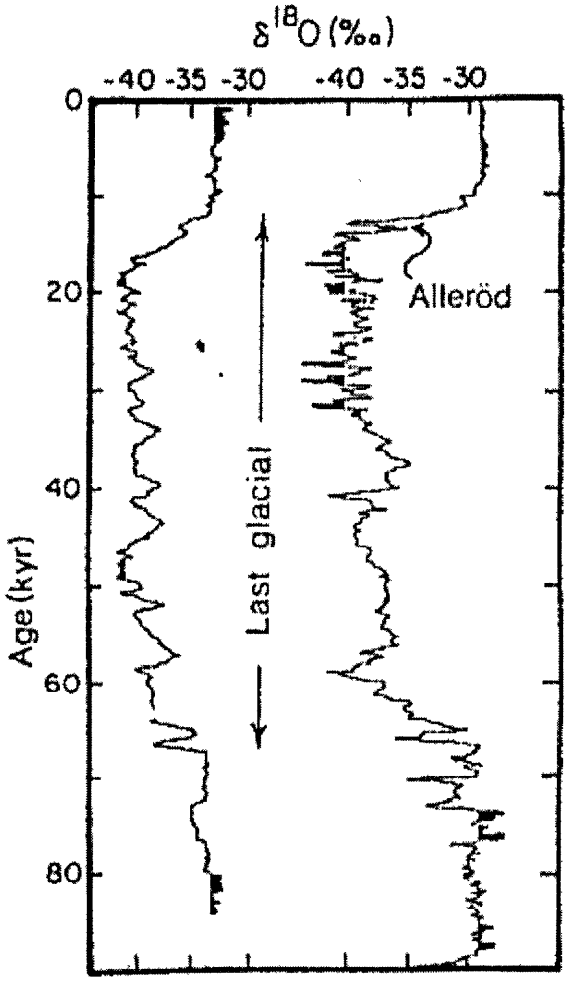

Figure 1-2: Reynaud et al. (1993) : CO_2 and $\delta^{18}O$ record

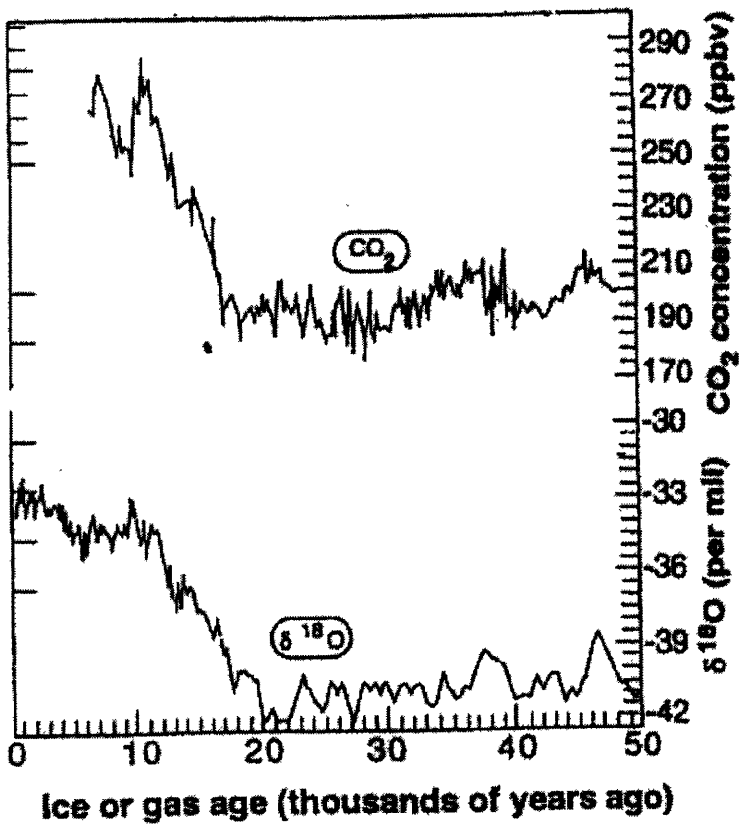

Figure 1-3: Siegenthaler and Sarmiento (1993) : Reserviors of CO_2

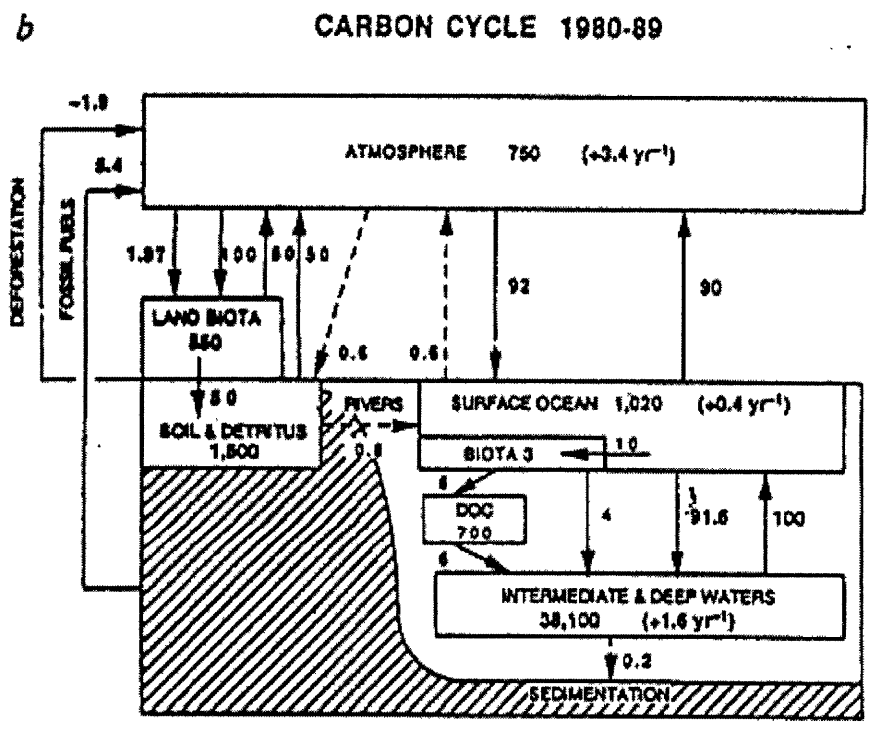

Figure 1-4: Manabe and Stouffer (1993) : Temporal Variation of Thermohaline Circulation

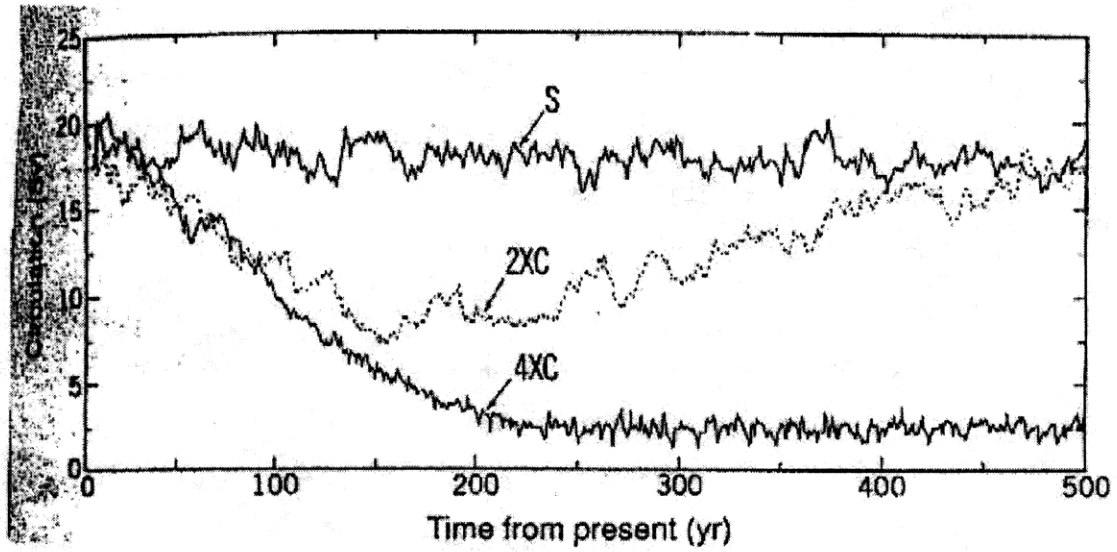

Chapter 2

Modeling Strategy

2.1 The atmosphere-ocean coupled system

This section briefly introduces the box model for the atmosphere-ocean coupled system, which provides the tool for investigating the atmosphere-ocean dynamics in this study. This model is based on the one developed by Marotzke (20,21). Figure 2-1 and 2-2 are schematic diagrams of the model. The model involves three boxes for the ocean and two boxes for the atmosphere. We assume that the area of the sea surface is the same between high and low latitudes. This model represents a single hemisphere or the perfectly symmetric Earth and the zonal average. Therefore, it represents the latitudinal and vertical transport only. Temperature and salinity are the primary dependent variables, and the independent variable is time in this model.

H is the depth of the ocean whereas h is the thickness of the surface layer. T_h, T_l, and T_d are the temperatures of high and low latitudes surface ocean and the deep ocean, and S_h, S_l, and S_d are the salinity. We assume that the heat capacity of the atmosphere is negligible compared to that of the ocean so that atmospheric mean temperature is instantly equilibrated with SST. H_h and H_l are the ocean heat gain through the surface, and H_{0h} and H_{0l} are the atmospheric energy gain at the top of the atmosphere. H_m is the meridional energy transport in the atmosphere. E is the net evaporation at low latitudes, and is also the net precipitation at high latitudes. F_m is the meridional atmospheric moisture transport.

To begin with, we can write down the conservation of heat (energy) and salinity in differential form.

$$\dot{T}_h = H_h + q(T_l - T_h) + K(T_d - T_h) \tag{2.1}$$

$$\dot{T}_l = H_l - q(T_l - T_d) \tag{2.2}$$

$$\dot{T}_d = \frac{h}{2(H-h)}\{q(T_h - T_d) - K(T_d - T_h)\} \tag{2.3}$$

$$\dot{S}_h = -H_s + q(S_l - S_h) + K(S_d - S_h) \tag{2.4}$$

$$\dot{S}_l = H_s - q(S_l - S_d) \tag{2.5}$$

$$\dot{S}_d = \frac{h}{2(H-h)}\{q(S_h - S_d) - K(S_d - S_h)\} \tag{2.6}$$

The dimension of equation 2.1, 2.2 and 2.3 is $[Ts^{-1}]$, so both sides of those equations can be multiplied by the heat capacity of water column, $c\rho_0 H \cdot (Area)$ to have the dimension of energy. We introduced a new variable q, which is the intensity of thermohaline circulation. Note that these relations holds only when $q > 0$ which signifies the thermally-driven high latitude sinking state. We assume that q is proportional to the buoyancy induced by temperature and salinity gradient with constant k.

$$q = k[\alpha(T_l - T_h) - \beta(S_l - S_h)] \tag{2.7}$$

K is the strength of the deep convection represented as a diffusive mixing. The model does diffusive mixing at the sinking surface ocean only, and K is set equal to $\mid q \mid$. Therefore, the equations 2.1 through 2.6 must be rewritten if it is in the salinity-driven low latitudes sinking state.

$$\dot{T}_h = H_h + \mid q \mid (T_d - T_h) \tag{2.8}$$

$$\dot{T}_l = H_l - \mid q \mid (T_l - T_h) + K(T_d - T_l) \tag{2.9}$$

$$\dot{T}_d = \frac{h}{2(H-h)}\{\mid q \mid (T_l - T_d) - K(T_d - T_l)\} \tag{2.10}$$

$$\dot{S}_h = -H_s + \mid q \mid (S_d - S_h) \tag{2.11}$$

$$\dot{S}_l = H_s - \mid q \mid (S_l - S_h) + K(S_d - S_l) \tag{2.12}$$

$$\dot{S}_d = \frac{h}{2(H-h)}\{\mid q \mid (S_l - S_d) - K(S_d - S_l)\} \tag{2.13}$$

Another new variable is H_s, which is the virtual salinity flux associated with the moisture transport by the atmosphere, E.

$$H_S = S_0 \frac{E}{H} \tag{2.14}$$

where S_0 is the characteristic salinity and H_S has H, the depth of the ocean, for its denominator. The atmosphere gains heat from solar radiation and loses heat by outgoing infrared radiation, so we parameterize the net heat exchange at the top of the atmosphere. When this AO model is integrated into the AOC model, these are the parameters affected by pCO_2 (1). CO_2 is one of the major greenhouse gases. CO_2 absorbs the outgoing infrared radiation and re-radiates back toward the surface of the earth. Therefore the higher pCO_2 is, the less heat escapes from the atmosphere while the incoming solar radiation remains constant. It results in a net increase in the radiation absorbed by the atmosphere. The relationship between pCO_2 and the change in A_h and A_l is logarithmic(1,22). Another words, an exponential growth of pCO_2 leads to a linear increase of A_h and A_l.

$$H_{0h} = A_h(pCO_2) - BT_h \tag{2.15}$$

$$H_{0l} = A_l(pCO_2) - BT_l \tag{2.16}$$

$$A_h(pCO_2) = A_{h0} + A_{h1} \log \frac{pCO_2}{pCO_2^{ref}} \tag{2.17}$$

$$A_l(pCO_2) = A_{l0} + A_{l1} \log \frac{pCO_2}{pCO_2^{ref}} \tag{2.18}$$

pCO_2^{ref} is taken near the current pCO_2. Here, the radiation balance is coupled to the the C model. We assume that H_m, which is the meridional energy transport in the atmosphere, can be written as a power function of the temperature gradient. F_m

can also be written as a power function of temperature gradient.

$$H_m = \tilde{\chi_n}(T_l - T_h)^n \qquad for \qquad n \geq 0 \tag{2.19}$$

$$F_m = \tilde{\gamma_m}(T_l - T_h)^m \qquad for \qquad m \geq 0 \tag{2.20}$$

This model assumes the linear relation $n = m = 1$ and $\tilde{\chi_n} = \tilde{\chi}, \tilde{\gamma_m} = \tilde{\gamma}$. Higher order m and n can be examined elsewhere. The conservation of heat in the atmosphere can be written as following.

$$F_{0h}H_{0h} - F_h\tilde{H}_h + H_m = 0 \tag{2.21}$$

$$F_{0l}H_{0l} - F_l\tilde{H}_l - H_m = 0 \tag{2.22}$$

where F_{0h} is the total area of the land and the ocean in high latitudes and F_h is the area of ocean only in high latitudes. Similarly, F_{0l} is the area of both of the land and the ocean in low latitudes and F_l is the area of the ocean. Combining 2.15, 2.16, 2.19, 2.21, and 2.22, we can eliminate H_{0h}, H_{0l}, and H_m, and obtain the H_h and H_l as functions of temperature.

$$\tilde{H}_h = \frac{1}{\varepsilon}(A_h - BT_h) + \frac{\tilde{\chi}}{\varepsilon F_{0h}}(T_l - T_h) \tag{2.23}$$

$$\tilde{H}_l = \frac{1}{\varepsilon}(A_l - BT_l) - \frac{\tilde{\chi}}{\varepsilon F_{0h}}(T_l - T_h) \tag{2.24}$$

where $\varepsilon \equiv \frac{F_h}{F_{0h}}$, $\tilde{H}_h \equiv H_h c\rho_0 H$ and $\tilde{H}_l \equiv H_l c\rho_0 H$. Using relationship 2.23 and 2.24, H_h and H_l can be eliminated from the equation 2.1 and 2.2 or 2.8 and 2.9. This is the complete preparation for integrating the temperature part of the AO model.

The salinity part of the model includes the virtual salinity flux, H_S, which is to be eliminated from the salinity balance equations, 2.4, 2.5, 2.11 and 2.12. We first look at the moisture balance in the atmosphere at high latitudes. Some fraction of

moisture transported from low latitudes precipitates on land at high latitudes and eventually goes back to low latitudes through rivers. We carefully parameterize the effect of rivers on the virtual salinity flux. We define E_W as the ratio between the precipitation which goes back to low latitudes ocean and the total precipitation at high latitudes. In original paper (21), it is the ratio of the catchment area to the total area.

$$EF_h = F_m E_W \tag{2.25}$$

We obtain H_S as a function of SST gradient by combining 2.20 and 2.25.

$$H_S = \frac{1}{E_W}\frac{S_0}{H}\gamma(T_l - T_h) \tag{2.26}$$

We also define ε_W to be the ratio of the catchment area to the ocean area and at high latitudes and $\gamma \equiv \frac{\tilde{\gamma}}{(oceanarea)}$. Finally, we eliminated H_S and the equation 2.1 through 2.6 and 2.8 through 2.13 become a set of six coupled ordinary differential equations (ODE). These ODEs completely determine the time evolution of the state of the AO system.

for $q > 0$

$$\dot{T}_h = \frac{1}{\varepsilon}(\frac{A_h - BT_h}{c\rho_0 H}) + \frac{\chi}{\varepsilon c\rho_0 H}(T_l - T_h) + q(T_l - T_h) + K(T_d - T_h) \tag{2.27}$$

$$\dot{T}_l = \frac{1}{\varepsilon}(\frac{A_l - BT_l}{c\rho_0 H}) - \frac{\chi}{\varepsilon c\rho_0 H}(T_l - T_h) - q(T_l - T_d) \tag{2.28}$$

$$\dot{T}_d = \frac{h}{2(H-h)}\{q(T_h - T_d) - K(T_d - T_h)\} \tag{2.29}$$

$$\dot{S}_h = -\frac{1}{E_W}\frac{S_0}{H}\gamma(Tl - Th) + q(S_l - S_h) + K(S_d - S_h) \tag{2.30}$$

$$\dot{S}_l = \frac{1}{E_W}\frac{S_0}{H}\gamma(Tl - Th) - q(S_l - S_d) \tag{2.31}$$

$$\dot{S}_d = \frac{h}{2(H-h)}\{q(S_h - S_d) - K(S_d - S_h)\} \tag{2.32}$$

for $q < 0$

$$\dot{T}_h = \frac{1}{\varepsilon}\left(\frac{A_h - BT_h}{c\rho_0 H}\right) + \frac{\chi}{\varepsilon c\rho_0 H}(T_l - T_h) + \mid q \mid (T_d - T_h) \tag{2.33}$$

$$\dot{T}_l = \frac{1}{\varepsilon}\left(\frac{A_l - BT_l}{c\rho_0 H}\right) - \frac{\chi}{\varepsilon c\rho_0 H}(T_l - T_h) - \mid q \mid (T_l - T_h) + K(T_d - T_l) \tag{2.34}$$

$$\dot{T}_d = \frac{h}{2(H-h)}\{\mid q \mid (T_l - T_d) - K(T_d - T_l)\} \tag{2.35}$$

$$\dot{S}_h = -\frac{1}{E_W}\frac{S_0}{H}\gamma(Tl - Th) + \mid q \mid (S_d - S_h) \tag{2.36}$$

$$\dot{S}_l = \frac{1}{E_W}\frac{S_0}{H}\gamma(Tl - Th) - \mid q \mid (S_l - S_h) + K(S_d - S_l) \tag{2.37}$$

$$\dot{S}_d = \frac{h}{2(H-h)}\{\mid q \mid (S_l - S_d) - K(S_d - S_l)\} \tag{2.38}$$

2.2 The global carbon cycle system

This section introduces the 4-box oceanic carbon cycle (C) model which is the tool for estimating the distribution of nutrients, dissolved inorganic carbons (DIC), and carbon dioxide in the atmosphere. It was developed by Follows(personal communication) and Figure 2-1 and 2-2 are the schematic diagrams for the model. The structure of the model is essentially similar to what is called the Harvardton Bear model whose name is taken from Harvard, Princeton and Bern Universities, the universities of the authors of three independent papers published almost at the same time (16,24). Follows and Marotzke modified the mathematical structure of the model and introduced the Newtonian damping formulation for the time evolution of the system. The model becomes quite clear and robust for understanding and exploring the behavior of the C system.

The notation of the parameters are to be consistent between the AO and the C model so that they are freely exchangeable when two models are coupled. The box model includes three well-mixed boxes of the ocean with depth H and a box of the atmosphere. Upper layer of the ocean boxes represent euphotic layer at low and high latitudes where photosynthesis takes place. The depth of euphotic layer is h and the depth of the entire ocean is H. The overturning circulation was prescribed as q

when uncoupled. The latitudinal extent of the ocean is $2\Delta y$, and is evenly divided by low and high latitudes. The longitudinal length of the ocean boxes is Δx. The model defines the concentration of nutrients at each boxes as N_h, N_l, and N_d for high latitudes, low latitudes, and the deep ocean. The model assumes vertical mixing to be parameterized as a diffusive process with the diffusive constant K. The expression for the conservation of nutrients is to be written as following.

for $q > 0$

$$\frac{d(N_h)}{dt} = -q(N_h - N_l) - K(N_h - N_d) - \lambda_h N_h \tag{2.39}$$

$$\frac{d(N_l)}{dt} = q(N_d - N_l) - \lambda_l N_l \tag{2.40}$$

$$\frac{d(N_d)}{dt} = \frac{h}{2(H-h)}\{q(N_h - N_d) + K(N_h - N_d) + \lambda_h N_h + \lambda_l N_l\} \tag{2.41}$$

for $q < 0$

$$\frac{d(N_h)}{dt} = -\mid q \mid (N_h - N_d) - \lambda_h N_h \tag{2.42}$$

$$\frac{d(N_l)}{dt} = \mid q \mid (N_h - N_l) - K(N_l - N_d) - \lambda_l N_l \tag{2.43}$$

$$\frac{d(N_d)}{dt} = \frac{h}{2(H-h)}\{\mid q \mid (N_l - N_d) + K(N_l - N_d) + \lambda_h N_h + \lambda_l N_l\} \tag{2.44}$$

where λ_h and λ_l are the rate of the export production of photosysthesis, which is determined by the incoming solar radiation and possibly other factors but they are prescribed in this model. The time evolution of the nutrient cycle is completely determined by integrating the set of ODEs.

The oceanic CO_2 uptake has two fundamental processes, which are the solubility and the biological pumps. The solubility pump refers to the oceanic CO_2 uptake through the exchange of gases between the ocean and the atmosphere. The aqueous concentration of a gas is determined by the partial pressure of the gas, SST, and SSS. A colder sea surface temperature yields a greater equilibrium concentration of gases. The biological pump refers to the oceanic CO_2 uptake through biological activity in the ocean. Photosynthesis by plankton consumes DIC and synthesizes organic carbon

molecules, some of which sink downwards in particulate form and dissolve again at deeper layers. The efficiency of the biological pump is controlled by the supply of solar radiation and nutrients. Nitrate and phosphate are regarded as two major limiting nutrients, out of which this model focus on nitrates. There could be other limiting nutrients but they are out of the scope of this research. The distribution of the limiting nutrients mainly depends on the physical mixing and the convective motion of the ocean.

The concentration of DIC are DIC_h, DIC_l, and $DIC_d[mol \cdot kg^{-1}]$ for high latitudes, low latitudes, and the deep ocean. The model assumes the total amount of carbon remains constant in the atmosphere and the ocean. The conservation of carbon in the system is to be written as following.

$$\overline{DIC} = \frac{h}{2H}(DIC_h + DIC_l) + \frac{H-h}{H}DIC_d \tag{2.45}$$

$$\overline{DIC} \cdot (2\rho H \Delta y \Delta x) + pCO_2^{at} \cdot \frac{M^{at}}{m} = constant \tag{2.46}$$

where $\frac{M^{at}}{m}[mol]$ is the ratio of the mass of atmosphere to the molecular mass of the air. $\overline{DIC}$ is the global mean DIC concentration. The time evolution of DIC and pCO_2 is not as simple as nutrients. It involves the air-sea exchange of CO_2 and the carbon chemistry in the sea water at the same time. The reactions of the carbon chemistry can be summarized as following.

$$CO_2(gas) \rightleftharpoons CO_2(aq) \tag{2.47}$$

$$CO_2(aq) + H_2O \rightleftharpoons H_2CO_3 \tag{2.48}$$

$$[CO_2] \equiv [CO_2(aq)] + [H_2CO_3] \tag{2.49}$$

$$H_2CO_3 \rightleftharpoons H^+ + HCO_3^- \tag{2.50}$$

$$HCO_3^- \rightleftharpoons H^+ + CO_3^{2-} \tag{2.51}$$

Since $[CO_2(aq)]$ and $[H_2CO_3]$ are almost indistinguishable, $[CO_2]$ is defined as a

sum of both species. The concentration of the total inorganic carbon in the system is the sum of $[CO_2]$, $[HCO_3^-]$, and $[CO_3^{2-}]$. I define ${k_1}^f$ as the rate of forward reaction in 2.50, and ${k_1}^b$ as the rate of backward reaction. Similarly, I define ${k_2}^f$ and ${k_2}^b$ as the rate of the forward and backward reaction in 2.51. Piston velocity, V_P, and the size of the ocean reservoir determines the time scale of air-sea exchange of gases. Following equations mean that the time change of $[CO_2]$ are proportional to the piston velocity, the inverse of the mixed layer thickness and the imbalance between the partial pressure of the ocean and the atmosphere. The air-sea CO_2 exchange is immediately followed by the production of bicarbonates and carbonates from $[CO_2]$. Therefore, the time change of $[CO_2]$ also depends on how fast $[CO_2]$ changes to the bicarbonate ion, $[HCO_3^-]$ and $[HCO_3^-]$ changes back to $[CO_2]$. The time change of $[HCO_3^-]$ and $[CO_3^{2-}]$ also depend on how fast they are created and destroyed in the chemical reaction.

$$\frac{d[CO_2]}{dt} = -\frac{V_P}{h}([CO_2] - [CO_2^*]) - {k_1}^f[CO_2] + {k_2}^b[H^+][HCO_3^-] \quad (2.52)$$

$$\frac{d[HCO_3^-]}{dt} = {k_1}^f[CO_2] - {k_1}^b[H^+][HCO_3^-] - {k_2}^f[HCO_3^-] + {k_2}^b[H^+][CO_3^{2-}] \quad (2.53)$$

$$\frac{d[CO_3^{2-}]}{dt} = {k_2}^f[HCO_3^-] - {k_2}^b[H^+][CO_3^{2-}] \quad (2.54)$$

Taking the sum of equations 2.52, 2.53 and 2.54 provides the time dependent equation for DIC. $[{CO_2}^{at}]$ is the product of the solubility,K_0 and $p{CO_2}^{at}$, which is the equilibrium value for $[CO_2]$.

$$\frac{dDIC}{dt} = -\frac{V_P}{h}([CO_2] - [CO_2]^{at}) \quad (2.55)$$

$$[CO_2]^{at} = K_0 \cdot pCO_2^{at} \quad (2.56)$$

Let us first concentrate on the equilibrium state here. The time dependent equation will be discussed later.

K_0 is known to be an emperical function of SST and SSS (30). Taking the steady states of 2.52, 2.53 and 2.54 give the equilibrium constant, K_1 and K_2.

$$[CO_2]_0 \doteq [CO_2{}^{at}] \tag{2.57}$$

$$K_1 = \frac{k_1{}^f}{k_1{}^b} = \frac{[H^+]_0[HCO_3^-]_0}{[CO_2]_0} \tag{2.58}$$

$$K_2 = \frac{k_2{}^f}{k_2{}^b} = \frac{[H^+]_0[CO_3^{2-}]_0}{[HCO_3^-]_0} \tag{2.59}$$

K_0, K_1 and K_2 are known as functions of SST and SSS emperically (12).

$$\begin{aligned} \ln K_0(T,S) \cong & -60.2409 + 93.4517(\frac{100}{T}) + 23.3585\ln(\frac{T}{100}) \\ & +S\{0.023517 - 0.023656(\frac{T}{100}) + 0.0047036(\frac{T}{100})^2\} \end{aligned} \tag{2.60}$$

$$\begin{aligned} pK_1 \cong & \frac{812.27}{T} + 3.356 - 0.00171S\ln T \\ & +0.000091S^2 \end{aligned} \tag{2.61}$$

$$\begin{aligned} pK_2 \cong & \frac{1450.87}{T} + 4.604 - 0.00385S\ln T \\ & +0.000182S^2 \end{aligned} \tag{2.62}$$

By combining K_1, K_2, and $[H^+]$, one can relate $[CO_2]$ to DIC at equilibrium.

$$DIC \equiv [CO_2] + [HCO_3^-] + [CO_3^{2-}] \tag{2.63}$$

$$DIC_0 = [CO_2]_0 \cdot (1 + \frac{K_1}{[H^+]_0} + \frac{K_1K_2}{[H^+]_0{}^2}) \tag{2.64}$$

$$= [CO_2]_0 \cdot R_C \tag{2.65}$$

$$= R_C K_0 \cdot pCO_2{}^{at} \tag{2.66}$$

The time dependent equation assumes that $[CO_2]$ is close to its equilibrium value. pCO_2, $[CO_2]$ and DIC can be written as a small perturbation from equilibrium value.

$$DIC = DIC_0 + DIC^* \tag{2.67}$$

$$[CO_2] = [CO_2]_0 + [CO_2]^* \tag{2.68}$$

$$pCO_2 = {pCO_2}^{at} + {pCO_2}^* \tag{2.69}$$

Inserting these relationship into the equation 2.55 can eliminate the constant term and leave perturbation terms only. The equation 2.55 involves both DIC and $[CO_2]$ but it is possible to rewrite it with a single variable.

$$\frac{dDIC^*}{dt} = -\frac{V_P}{h} \cdot [CO_2]^* \tag{2.70}$$

Revelle factor represents the ratio of the rate of change between pCO_2 and DIC, which normally remains within 8 to 12 in the ocean. Here, the relation can be applied to the conversion of variables for Equation 2.55.

$$\frac{{pCO_2}^*}{pCO_{20}} \cong B \cdot \frac{DIC^*}{DIC_0} \tag{2.71}$$

$${pCO_2}^* \cong B\frac{pCO_{20}}{DIC_0} \cdot DIC^* \tag{2.72}$$

$${pCO_2}^* \cong \frac{B}{K_0 R_C} \cdot DIC^* \tag{2.73}$$

$$[CO_2]^* \cong \frac{B}{R_C} \cdot DIC^* \tag{2.74}$$

Applying Equation 2.74 to 2.70,

$$\frac{dDIC^*}{dt} \cong -\frac{V_P B}{h R_C} \cdot DIC^* \tag{2.75}$$

$$\frac{dDIC}{dt} \cong -\frac{V_P B}{h R_C} \cdot (DIC - DIC_0) \tag{2.76}$$

R_C reflects the chemistry of bicarbonates and carbonates, which is essentially non-linear. Here, I introduce a simplifed parametrization for R_C, which is a lin-

earized solution for the non-linear full carbon equations. The linearlized R_C makes the stepping-forward calculation much faster than the iterative method. It also gives a clear insight to how the carbon chemistry reacts to perturbations in SST, SSS and DIC. The simplified expression is an extremely powerful tool to explore the interaction between the dynamics and chemistry of carbon cycle.

According to Equation 2.64 and 2.65, R_C is completely determined if K_1, K_2 and $[H^+]$ are given. SST and SSS can determine K_1 and K_2 but $[H^+]$ remains unknown. $[H^+]$ or pH is influenced by different species of ions in the sea water including bicarbonates and carbonates. The system needs to have another condition to explicitly solve for pH. The total alkalinity, Alk, is the frequently used quantity to solve this problem. Alk is the sum of electric charges from all the strong ions in the sea water.

$$Alk \equiv [Na^+] + 2[Mg^{2+}] - [Cl^-] + [K^+] + 2[Ca^{2+}] + (other\ \ strong\ \ ions) \quad (2.77)$$

The electrically neutral ocean requires that the alkalinity has to be balanced by the negative charges of weak ion species.

$$Alk \cong [HCO_3^-] + 2[CO_3^{2-}] + [OH^-] - [H^+] \quad (2.78)$$

If alkalinity is an externally given parameter and SST, SSS, and DIC are also given, one can solve 2.61, 2.62, 2.64 and 2.78 to obtain pH. The equation becomes nonlinear and it is usually solved through iteration.

$$R_C \equiv 1 + \frac{K_1}{[H^+]} + \frac{K_1 K_2}{[H^+]^2} \quad (2.79)$$

$$Alk \cong [CO_2]_0 \left(\frac{K_1}{[H^+]} + \frac{2K_1K_2}{[H^+]^2}\right) + \frac{K_W}{[H^+]} - [H^+] \quad (2.80)$$

$$= \frac{DIC_0}{R_C}\left(\frac{K_1}{[H^+]} + \frac{2K_1K_2}{[H^+]^2}\right) + \frac{K_W}{[H^+]} - [H^+] \quad (2.81)$$

In this study the alkalinity is considered to be either a simple function of SSS

or just a constant. The surface alkalinity can be a linear function of SSS because both SSS and Alk are mainly controlled by evaporation and precipitation at surface according to Brewer et al (4,11).

$$Alk \cong 547.05 + 50.560S[\mu eq/kg] \tag{2.82}$$

The total alkalinity could be alternatively set equal to 2317 $[\mu eq/kg]$. Equation 2.81 provides fifth order polynomical of $[H^+]$, which is to be equated with either Equation 2.82 or 2317 $[\mu eq/kg]$. When Equation 2.82 is used, the system is to be called variable alkalinity model, whereas the constant alkalinity model sets the alkalinity to be equal to 2317 $[\mu eq/kg]$.

$$547.05 + 50.560S = \frac{DIC}{R_C}\left(\frac{K_1}{[H^+]} + \frac{2K_1K_2}{[H^+]^2}\right) + \frac{K_W}{[H^+]} - [H^+] \tag{2.83}$$

$$2317 = \frac{DIC}{R_C}\left(\frac{K_1}{[H^+]} + \frac{2K_1K_2}{[H^+]^2}\right) + \frac{K_W}{[H^+]} - [H^+] \tag{2.84}$$

$$\tag{2.85}$$

By giving proper values for SST, SSS and DIC, Equations 2.83 and 2.84 can be solved for $[H^+]$ through iterative method. Once pH is calculated, one can also calculate R_C using the $[H^+]$. However, different assumptions on alkalinity lead different results for R_C. I obtained pH and R_C for various SST, SSS and DIC in Figure 2-3, 2-4 and 2-5. The circular dots indicates the iterative solutions for the K_0R_C, and the solid line is the linear regression of the explicit solutions. The approximation does not give the perfect fit, but it does captures the basic behavior of the system. $K_0 \cdot R_C(T, S, DIC)$ is the only parameter which is involved in the equation of the system 2.87 through 2.92. (T_0, S_0, DIC_0) is reference values for SST, SSS and DIC, from which K_0R_C was linearly expanded. Solid straight lines shown in the Figure 2-3, 2-4 and 2-5 are the least-square linear expansion around the latitudional mean, $(15°C, 35‰_0, 2100\mu M)$. In the AOC model, I used the least-square linear expansion around $(5°C, 35‰_0, 2100\mu M)$ for high latitudes and $(25°C, 35‰_0, 2100\mu M)$ for low

latitudes. The results are shown in Table 2.1 and 2.2. The approximation becomes quite accurate when different sets of parameters are used for high and low latitudes.

$$K_0 \cdot R_C = a_0 + a_T(T - T_0) + a_S(S - S_0) + a_{DIC}(DIC - DIC_0) \tag{2.86}$$

The four coefficients, a_0, a_T, a_S, and a_{DIC}, describes fundamental feature of the carbon chemistry in the sea water. The next chapter explores the meaning of this parameterization in detail.

The time dependent equations for DIC in each of the ocean boxes includes the advective and diffusive mixing terms and the biological production terms in addition to the air-sea exchange of CO_2. Combining them together, the ODEs for DIC becomes following.

for $q > 0$

$$\begin{aligned}
\frac{d}{dt}(DIC_h) &= -q(DIC_h - DIC_l) - K(DIC_h - DIC_d) - \mu(DIC_h - DIC_h^*) \\
&\quad -r_{CN}\lambda_h N_h \qquad (2.87)\\
\frac{d}{dt}(DIC_l) &= q(DIC_d - DIC_l) - \mu(DIC_l - DIC_l^*) - r_{CN}\lambda_l N_l \qquad (2.88)\\
\frac{d}{dt}(DIC_d) &= \frac{h}{2(H-h)}\{q(DIC_h - DIC_d) + K(DIC_h - DIC_d) + r_{CN}\lambda_h N_h \\
&\quad +r_{CN}\lambda_l N_l\} \qquad (2.89)
\end{aligned}$$

for $q < 0$

$$\begin{aligned}
\frac{d}{dt}(DIC_h) &= -\mid q \mid (DIC_h - DIC_d) - \mu(DIC_h - DIC_h^*) - r_{CN}\lambda_h N_h \qquad (2.90)\\
\frac{d}{dt}(DIC_l) &= \mid q \mid (DIC_h - DIC_l) - K(DIC_l - DIC_d) - \mu(DIC_l - DIC_l^*) \\
&\quad -r_{CN}\lambda_l N_l \qquad (2.91)\\
\frac{d}{dt}(DIC_d) &= \frac{h}{2(H-h)}\{\mid q \mid (DIC_l - DIC_d) + K(DIC_l - DIC_d) + r_{CN}\lambda_h N_h \\
&\quad +r_{CN}\lambda_l N_l\} \qquad (2.92)
\end{aligned}$$

Figure 2-1: The schmatic diagram of the high latitudes sinking state

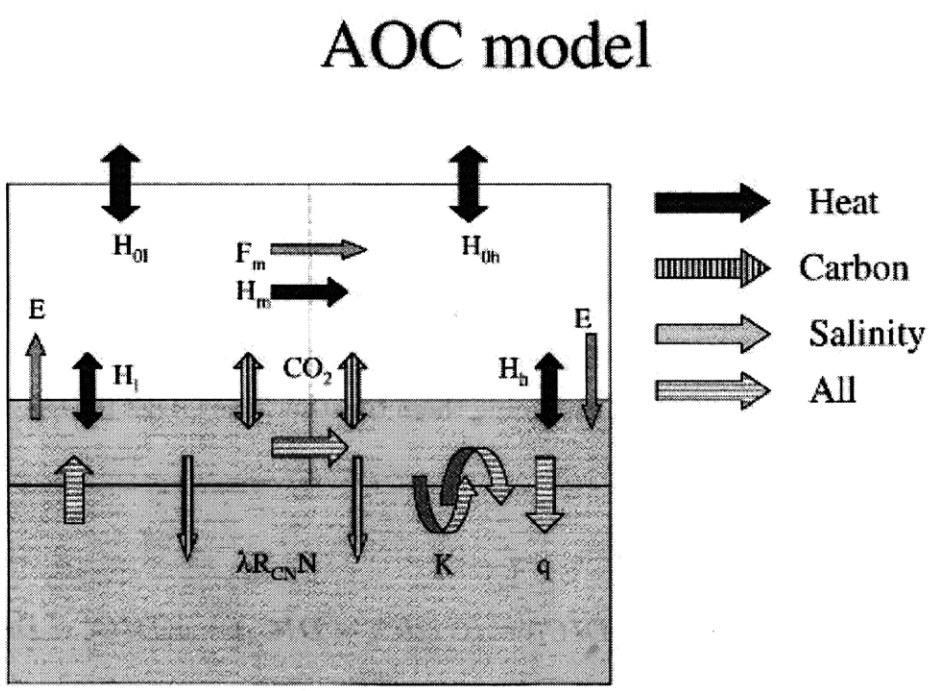

where $\mu \equiv \frac{V_P B}{h R_C}$ and r_{CN} is the Redfield ratio of carbon and nitrate which is assumed to be the limiting nutrients in this model. At this point, all the ODEs for the AOC models are introduced. The ODEs for the AO model are 2.27 through 2.38, and the ODEs for the C model is 2.39 through 2.44 and 2.87 through 2.92. Putting them altogether, the system contains twelve ODEs which can completely determine the time evolution of the AOC system.

Figure 2-2: The schmatic diagram of the low latitudes sinking state

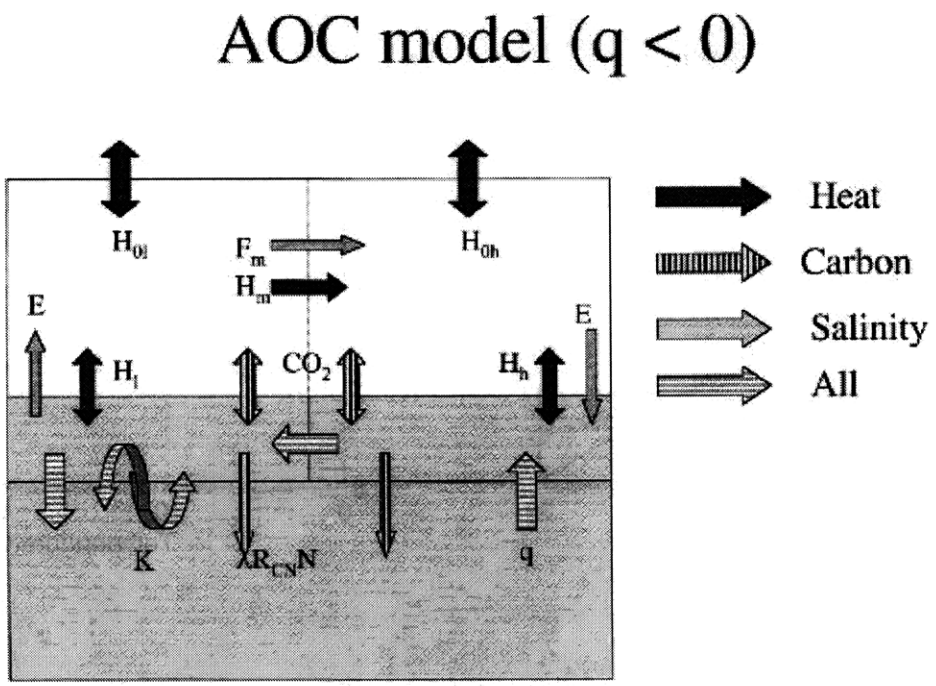

Table 2.1: Parameters for $K_0 \cdot R_C$: Variable Alk model

	a_0	a_T	a_{DIC}	a_S	T_0(C)	S_0(‰)	DIC_0(μ M)	σ^2
High lat.	12.77	-0.6589	-0.0695	2.889	5	35	2100	1.06
Low lat.	4.964	-0.1934	-0.0262	1.091	25	35	2100	0.166
Mean	8.014	-0.3846	-0.0413	1.720	15	35	2100	0.677

Table 2.2: Parameters for $K_0 \cdot R_C$: Fixed Alk model

	a_0	a_T	a_{DIC}	a_S	T_0(C)	S_0(‰)	DIC_0(μ M)	σ^2
High lat.	12.28	-0.6589	-0.0695	-0.2172	5	35	2100	0.110
Low lat.	4.770	-0.1934	-0.0262	-0.0822	25	35	2100	0.016
Mean	7.408	-0.3463	-0.0413	-0.1298	15	35	2100	0.510

Figure 2-3: $K_0 \cdot R_C$ and its estimate with variable T

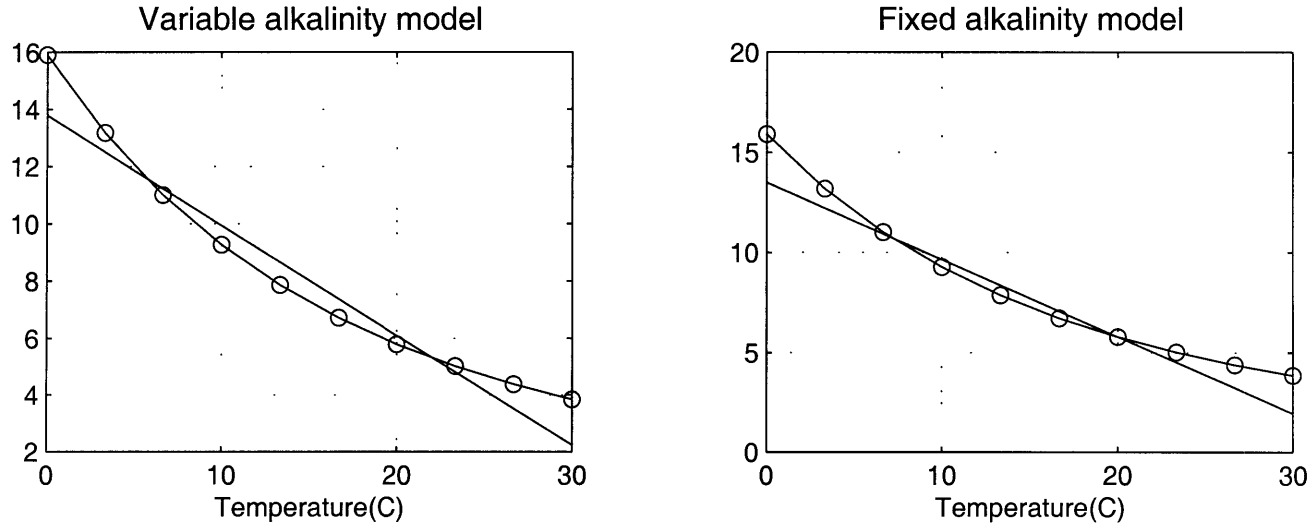

Figure 2-4: $K_0 \cdot R_C$ and its estimate with variable S

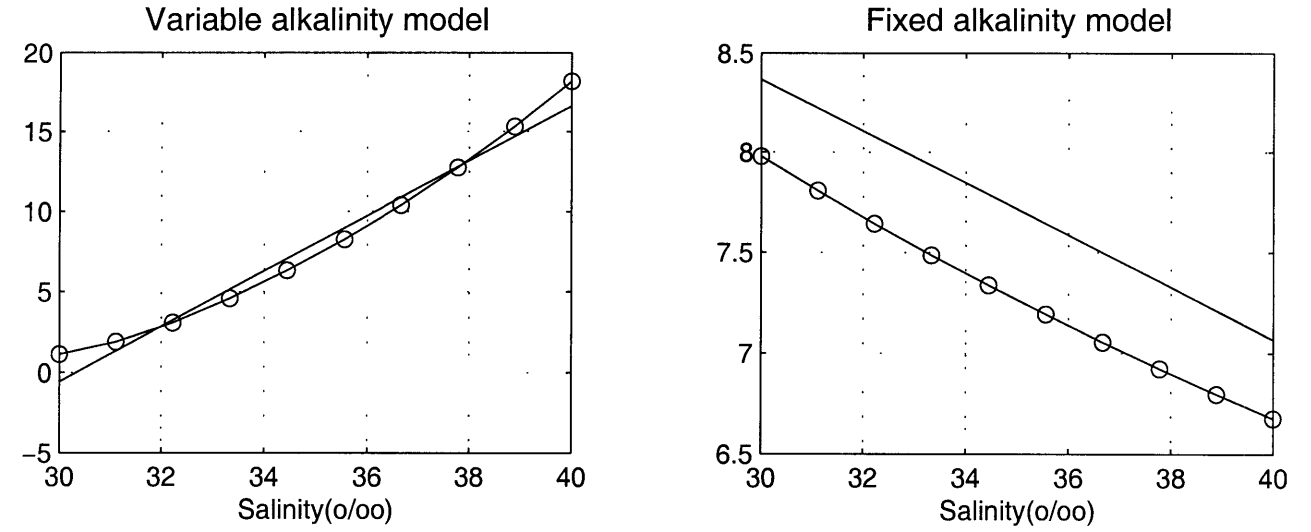

Figure 2-5: $K_0 \cdot R_C$ and its estimate with variable DIC

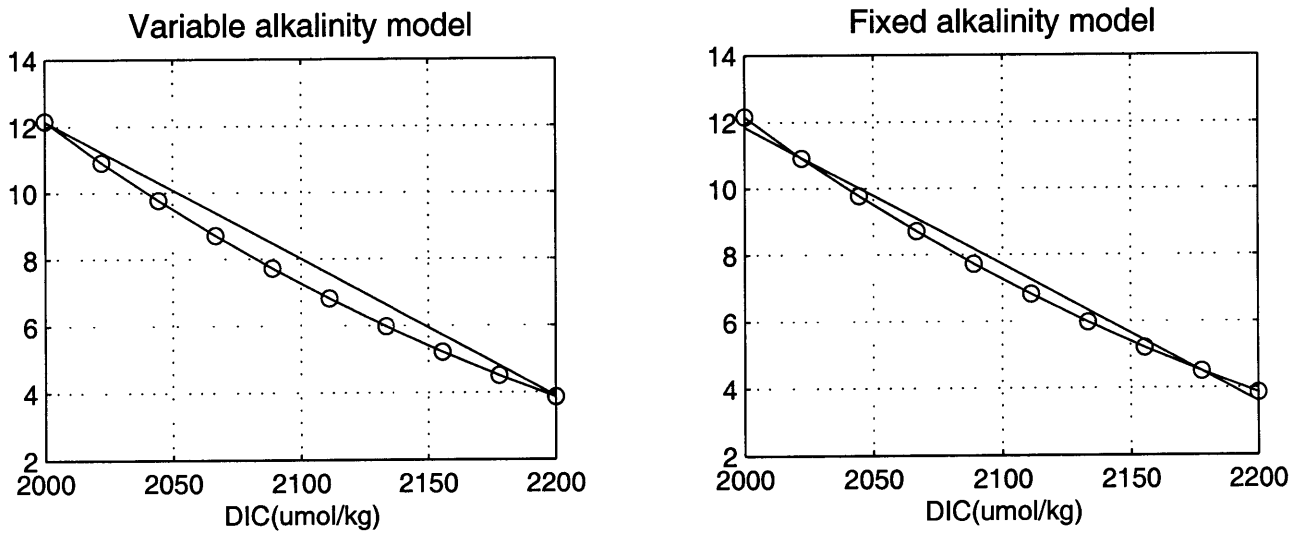

Chapter 3

Steady states

This chapter shows several important results of the numerical experiments specifically associated with the steady states of the system. The AOC model, introduced in the previous chapter, was put into computer codes and numerically integrated the time evolution of the AOC system with various initial conditions. The fundamental model parameters are shown in Table 3.1.

There are some different versions of the AOC model depending on how it couples the AO model and the C model. The comparison of the results between various conditions reveals interesting characteristic of the system. Figure 3-1 shows the structure of the AOC models. The coupled AOC system includes two basic subsystems which are the AO system and the C system. The AO system provides the dynamics of the system to the C system and the C system in turn feedbacks on the AO system through the radiation balance.

The fully-coupled AOC model includes all interactions between the AO system and the C system. The AO and the C models are fully interactive, thereby, it has the smallest number of prescribed parameters.

The fully-coupled AOC model :

$$\boxed{\mathrm{AO} \rightleftharpoons \mathrm{C}}$$

The fully-coupled model is the most complicated model and needs to be compared with simpler versions of the model to understand the feedback mechanism. The "semi-coupled model" also calculates the AO and the C model jointly but the interaction is one-directional. The C model is calculated based on the AO model at each time step but the C model does not affect the AO model at all. Therefore, it produces the same dynamics as the uncoupled AO model does, but the C system of the model does not feedback on the AO system.

The semi-coupled AOC model :

$$\boxed{\mathrm{AO} \rightarrow \mathrm{C}}$$

By comparing the fully-coupled and semi-coupled models, one can understand that the steady states of the AOC system are basically determined by the AO system. It also helps to estimate the importance of the feedback between the AO and the C part of the model. The uncoupled C model is also examined in this chapter. It is the simplest model in this study. It takes SST and SSS given as external conditions. Each version of the AOC models uses exactly the same parameters shown in the Table 3.1. The total amount of carbon and nutrient in the system is also kept constant throughout the model runs in this study. Differences among the various model runs are solely based on the difference in initial conditions in temperature and salinity of the ocean or the difference in the method of the coupling of subsystems. The table 3.2 shows the standard set of initial conditions for the AOC model runs.

3.1 The fully coupled AOC model

The model has two steady state solutions. These two steady states are the characteristic behavior of the AO model (21). One is, the temperature-driven, high latitude sinking (HS) mode and the other is, the salinity-driven, low latitude sinking (LS) mode. The AOC model results in the HS mode when the initial condition is similar to the current climate. In order for the system to take the LS mode, the high latitude

ocean must have very low salinity compared to the current climate.

It takes several thousand years for the AOC model to reach its steady states. pCO_2 = 261.4(ppmv) in the HS mode at equilibrium. In contrast, pCO_2 = 536.7(ppmv) in LS mode. Table 3.3 shows the rest of parameters. The global mean temperature is different by only 2.8° C between the HS and the LS modes but the pCO_2 is different by 275 ppmv.

BIO is the biological export production at the surface layer, which is often called the particulate flux. It is about 0.9 $molC \cdot m^{-2} \cdot yr-1$ at both low and high latitudes in the HS mode. The LS mode has very weak biological activity at high latitudes compared to the HS mode. The stratification of the mixed layer causes depleted nitrates at the high latitudes, and results in the weak biological activity.

Int.H.Trans represents the interhemispheric transport of carbons, which is the amount of carbons transported from high latitudes to low latitudes through the deep ocean. The negative sign means the reverse direction, which is low latitudes from high latitudes.

The two steady states have very different thermohaline intensity. The thermohaline circulation is very weak in the LS mode. Interestingly, the low latitude surface layer has higher DIC concentration in the LS state. It is because of the effect of the high alkalinity associated with the salinity. It will be discussed in detail in the section 3.4.

Most of these characteristics are not obvious. It is necessary to take a look at the simpler models to understand what is actually making the difference between the HS and the LS modes.

3.2 The semi-coupled AOC model

The list of the output of the semi-coupled model is in Table 3.4. The mean temperature is the same between the HS and the LS modes because pCO_2 does not affect the radiation balance in the semi-coupled model. The thermihaline circulation does not change the global mean temperature directly according to the previous study (21).

The net incoming radiation, A_h and A_l, depends on atmospheric pCO_2 in Equation 2.17 and 2.18. The semi-coupled model sets pCO_2 equal to $pCO_2{}^{ref}$ so that the radiative forcing remains the same between the HS and the LS mode.

It is remarkable that pCO_2 increased in the HS mode and decreased in the LS mode compared to the fully-coupled outcome, so the difference in pCO_2 reduced to 216 ppmv in the semi-coupled model.

The comparison of the global mean temperature :

Mode	Semi-coupled		Fully-coupled
HS	15.3° C	$\longrightarrow$	14.3° C
LS	15.3° C	$\longrightarrow$	17.1° C
Difference	0° C	$\longrightarrow$	2.8° C

The comparison of pCO_2 :

Mode	Semi-coupled		Fully-coupled
HS	280 ppmv	$\longrightarrow$	261 ppmv
LS	496 ppmv	$\longrightarrow$	537 ppmv
Difference	216 ppmv	$\longrightarrow$	276 ppmv

In the semi-coupled model, the global mean temperature (T_M) is warmer in the HS mode and cooler in the LS mode than those of the fully-coupled model. There is a clear correlation between the temperature and pCO_2. The low pCO_2 leads to a relatively cool climate in the HS mode when it is fully-coupled. A cool SST increases the solubility of the CO_2 in the sea water so that the ocean takes up more CO_2 and leaves even less CO_2 in the atmosphere. On the other hand, a high pCO_2 raises the T_M in the LS mode. It reduces the solubility and results in the even higher concentration of CO_2 in the atmosphere. This positive feedback, the self-amplifying effect, is to be called the global warming feedback. The next chapter, 4, will examine several feedback mechanisms in detail including the global warming feedback.

The semi-coupled model filters out the global warming feedback and any other feedbacks between the AO and the C model, but there is a significant difference

in pCO_2 between the HS and the LS mode. It implies that the carbon cycle is fundamentally different between the HS and the LS modes. Even though the T_M is the same, the pCO_2 is still different by 216 ppmv. The gradient of SST and SSS are different between the HS and LS modes, which leads to different circulation direction and intensity. They also affect the chemical property of the sea water. The intensity of the ocean circulation affects the rate of outgassing and the supply of nutrients to the surface. The direction of the circulation determines the outcropping surface. The system is quite complicated and there is a need to separate different effects using a simpler model. The next section discusses the uncoupled C model which can separate those different effects and is able to estimate the relative importance among them.

3.3 The uncoupled C model

3.3.1 What determines pCO_2 of the steady states?

The fact that both the fully coupled model and the semi-coupled model reached similar steady states implies that the AO part of the model primarily determines the dynamical behavior of the system. The C model has some impact on the AO model through the global warming feedback but the feedback does not involve the thermohaline circulation in absence of the Clausius-Clapeyron relationship, which will be discussed in the chapter 4. The C model passively determines the carbon cycle with a set of parameters for SST, SSS, and q which are provided by the AO model.

The gradient of SST and SSS determined the direction and the intensity of thermohaline circulation. In chapter 2, q was defined to be the parameter for the thermohaline circulation. The sign of q represents the direction (positive $\rightarrow$ HS) and the magnitude of q means the intensity. This q is determined by the gradient of SST and SSS according to 2.7. In the uncoupled C model, steady state solutions can be easily calculated through the analytical solution provided the information about SST, SSS, q and K. Follows previously solved the stationary solutions of the C model, and the solution provides several important characteristic of the steady states. The steady

state solution can be obtained from Equation 2.87 through 2.92 by setting left-hand side of the equations to zero.

For $q > 0$,

$$DIC_h{}^{eq} \cong DIC_h{}^* = K_0 R_{Ch} \cdot pCO_2{}^{at} \tag{3.1}$$

$$DIC_l{}^{eq} \cong DIC_l{}^* = K_0 R_{Cl} \cdot pCO_2{}^{at} \tag{3.2}$$

$$DIC_d{}^{eq} = DIC_h{}^* + \frac{\lambda_h r_{CN} N_h + \lambda_l r_{CN} N_l}{q + K} \tag{3.3}$$

For $q < 0$,

$$DIC_h{}^{eq} \cong DIC_h{}^* = K_0 R_{Ch} \cdot pCO_2{}^{at} \tag{3.4}$$

$$DIC_l{}^{eq} \cong DIC_l{}^* = K_0 R_{Cl} \cdot pCO_2{}^{at} \tag{3.5}$$

$$DIC_d{}^{eq} = DIC_l{}^* + \frac{\lambda_h r_{CN} N_h + \lambda_l r_{CN} N_l}{\mid q \mid + K} \tag{3.6}$$

Once DIC_h, DIC_l and DIC_d are determined, pCO_2 can be calculated from 2.46. In fact, DIC_d alone can approximate the atmospheric pCO_2 because the size of the deep ocean as a reservoir of CO_2 is by far larger than that of surface ocean.

$$pCO_2 \cong \frac{m^{at}}{M^{at}} \{constant - DIC_d(2\Delta x \Delta y H \rho)\} \tag{3.7}$$

The "constant" is the total amount of carbon in the system, which is kept constant throughout all model runs. The deep ocean DIC determines the pCO_2 of the steady states. The deep ocean DIC is determined by the combination of SST and SSS of the sinking surface ocean and the magnitude of q and K. The sign of q determines the outcropping ocean through which the deep ocean outcrops CO_2. K is set equal to q in this study. Figure 3-2 shows the system behavior of the semi-coupled model. It provides the first-order approximate behavior of the AOC system because the fully-coupled and the semi-coupled model result in similar steady states.

The AO system determines SSS, SST, and the sign and the direction of the ther-

mohaline circulation. The C system determines the atmospheric pCO_2 based on the parameters. The SST, SSS, and the direction and the intensity of the thermohaline circulation are different between the HS and the LS modes. This section examines the importance of each parameters and attempts to elucidate what is causing the difference in the steady state pCO_2 between the HS and the LS mode. The uncoupled C model is free from the coupling of SST, SSS and q because they are all prescribed in this model. Therefore, the C model can estimate the relative importance among the parameters by breaking relationships between them.

3.3.2 The $\mid q \mid$ effect

The effect of the magnitude of q can be examined by fixing SST and SSS and varying the magnitude of q in the uncoupled model. The thermohaline intensity, $\mid q \mid$ was changed from 5.32 (S_V) to 53.2 (S_V) without changing the SST and SSS profiles based on the steady state HS mode. In the LS mode, $\mid q \mid$ was also changed from -26.6 (S_V) to -160 (S_V). The results of the model runs are following:

The comparison of model runs with various q :

Mode	q	pCO_2	BIO_h	BIO_l	Int.H.Trans
HS	5.32 S_V	259 ppmv	0.20	0.34	0.26 GTC$\cdot$ yr^{-1}
HS	13.3 S_V	266 ppmv	0.48	0.77	0.67 GTC$\cdot$ yr^{-1}
HS	26.6 S_V	280 ppmv	0.88	1.37	1.37 GTC$\cdot$ yr^{-1}
HS	39.9 S_V	295 ppmv	1.22	1.82	8.64 GTC$\cdot$ yr^{-1}
HS	53.2 S_V	308 ppmv	1.52	2.21	13.8 GTC$\cdot$ yr^{-1}
LS	-26.6 S_V	499 ppmv	0.93	1.08	-1.75 GTC$\cdot$ yr^{-1}
LS	-160 S_V	532 ppmv	3.85	2.93	- 14.2 GTC$\cdot$ yr^{-1}

The unit for BIO is $mol \cdot m^{-2} \cdot yr^{-1}$. The time scale for the system to reach its equilibrium becomes shorter as $\mid q \mid$ increases. A strong overturning circulation makes the deep ocean respond rapidly to the perturbation at the surface.

Intensifying thermohaline circulation moderately increases pCO_2 in all cases. Both the biological export production and the interhemispheric transport of carbons are

greatly increased by intensifying $\mid q \mid$. The enhanced biological activity tends to reduce pCO_2 through removing DIC from the surface mixed layers. However, the pCO_2 rises with a moderate rate ($< 25\%$) while the BIO increased much more than 1500%. It implies that there are competing processes in the system. Figure 3-3 is a schematic diagram of the competing processes. Increasing $\mid q \mid$ is analogous to speeding up the conveyor belt of DIC and nutrients in the ocean. Stronger overturning circulation well mixes the surface and the deep ocean. On one hand, it speeds up the rate of transporting DIC from the deep ocean to the surface mixed layer. The increased surface DIC releases CO_2 into the atmosphere and raises pCO_2. It is called the outgassing effect. On the other hand, it makes the biological pump very effective through supplying extra nutrients to the surface. Thereby, it transports DIC back into the deep ocean. These two separate processes take place at the same time and the net flux of CO_2 tends to remain within a narrow range according to the model runs.

Analytical calculation supports the numerical results. Equation 3.3 and 3.6 shows the steady state DIC for the deep ocean, which predominantly determines the atmospheric pCO_2. DIC_d is determined by N_h, N_h and DIC_h if it is in the HS mode. In the LS mode, N_h, N_h and DIC_l determine DIC_d. The steady state solution for nitrate can be obtained from Equation 2.39 through 2.44.

For $q > 0$,

$$N_l{}^{eq} = \frac{1}{1+\frac{\lambda_l}{q}} N_d \tag{3.8}$$

$$\cong \frac{q}{\lambda_l} N_d \quad for\ 1 \gg \frac{\lambda_l}{q} \tag{3.9}$$

$$N_h{}^{eq} = \frac{1}{1+\frac{K}{q}+\frac{\lambda_h}{q}} (N_l + \frac{K}{q} N_d) \tag{3.10}$$

$$\cong \frac{1}{2+\frac{\lambda_h}{q}} (N_l + N_d) \tag{3.11}$$

$$\cong \frac{q}{\lambda_h} N_d \quad for\ 2 \gg \frac{\lambda_h}{q} \tag{3.12}$$

For $q < 0$,

$$N_h{}^{eq} = \frac{1}{1+\frac{\lambda_h}{|q|}} N_d \tag{3.13}$$

$$\cong \frac{|\,q\,|}{\lambda_h} N_d \quad for\ \ 1 \gg \frac{\lambda_h}{|\,q\,|} \tag{3.14}$$

$$N_l{}^{eq} = \frac{1}{1+\frac{K}{|q|}+\frac{\lambda_l}{|q|}} (N_l + \frac{K}{|\,q\,|} N_d) \tag{3.15}$$

$$\cong \frac{1}{2+\frac{\lambda_l}{|q|}} (N_h + N_d) \tag{3.16}$$

$$\cong \frac{|\,q\,|}{\lambda_l} N_d \quad for\ \ 2 \gg \frac{\lambda_l}{|\,q\,|} \tag{3.17}$$

The scale of the magnitude of q is around 10^{-2} whereas the scale of λ is around 10^0. Therefore, the concentration of nitrate at the surface ocean is approximately proportional to the intensity of thermohaline circulation. Inserting the Equation 3.8 through 3.13 to 3.3 and 3.6, the steady state solution for the deep ocean DIC becomes independent of the intensity of the thermohaline circulation. It implies that the outgassing effect and the biological export production almost completely cancel out each other. Figure 3-3 presents the strong compensation effect between the two effects.

$$DIC_d{}^{eq} \cong DIC_h + r_{CN} \cdot N_d \quad HS\ \ mode \tag{3.18}$$

$$DIC_d{}^{eq} \cong DIC_l + r_{CN} \cdot N_d \quad LS\ \ mode \tag{3.19}$$

Another similar set of model runs are calculated based on constant nitrate concentration. This constant Biota model prescribes the concentration of nutrients for each ocean box no matter what $|\,q\,|$ is. It separates the effect of the biological pump from the pure effect of ocean DIC transportation. The constant Biota model ignores the nutrient cycle, thereby it underestimates the compensation between the outgassing effect and the biological pump.

The comparison of inorganic model runs with various q :

Mode	q	pCO_2	BIO_h	BIO_l	Int.H.Trans
HS	5.32 S_V	29.3 ppmv	0.85	0.96	1.10 GTC$\cdot$ yr^{-1}
HS	13.3 S_V	122 ppmv	0.85	0.96	1.41 GTC$\cdot$ yr^{-1}
HS	21.3 S_V	226 ppmv	0.85	0.96	1.56 GTC$\cdot$ yr^{-1}
HS	26.6 S_V	295 ppmv	0.85	0.96	1.22 GTC$\cdot$ yr^{-1}
HS	26.6 S_V	361 ppmv	0.85	0.96	1.29 GTC$\cdot$ yr^{-1}
HS	39.9 S_V	460 ppmv	0.85	0.96	1.13 GTC$\cdot$ yr^{-1}
HS	53.2 S_V	580 ppmv	0.85	0.96	

The change in pCO_2 is quite dramatic in the constant Biota models. Regardless of the existence of the biological pump, it turns out that the intensified thermohaline circulation increases pCO_2. But the rates of pCO_2 increase are quite different. Figure 3-4 shows that the rate of increase is suppressed in the standard C model by the biological activity. It is a limiting case of the Equation 3.3 and 3.6. The deep ocean DIC is inversely proportional to the intensity of the thermohaline circulation because nitrate concentration is fixed at the prescribed value. It results in the rapid increase in pCO_2 with a constant increase in q. The intensity of thermohaline circulation perturbs the carbon cycle strongly but the net effect on atmospheric pCO_2 is suppressed to some extent because the perturbation cancels out within the uncoupled C model.

3.3.3 The SSS SST and q effect

The previous section showed that the magnitude of q does not affect the steady state pCO_2 very much because the outgassing effect and the biological pump compensate each other. It is SST, SSS and the sign of q that primarily determine the atmospheric pCO_2 at the steady states. Whichever surface layer is sinking, the SST, SSS and DIC of the sinking layer dominate the property of the deep ocean. Equation 3.18 and 3.22 shows that the deep ocean DIC is completely determined by the property of the sinking surface ocean. The sign of q is critically important to the system because the sinking surface layer determines the fundamental property of the deep ocean.

The sinking surface layer is often referred as the outcropping ocean. $K_0 R_C$ is the parameter which determines the property of the surface ocean, and the previous chapter introduced a linearized parameterization for $K_0 \cdot R_C$ in the equation 2.86. The steady state pCO_2 can be obtained by following procedure. The outcropping ocean determines the deep ocean DIC with Equation 3.18 and 3.22. Given the deep ocean DIC, Equation 3.7 can solve for pCO_2.

$$
\begin{aligned}
DIC_d^{eq} &\cong pCO_2 \cdot K_0 R_{Ch} \cdot + r_{CN} \cdot N_d \quad HS \ mode && (3.20)\\
pCO_2 &\cong \frac{m^{at}}{M^{at}}\{constant - (pCO_2 \cdot K_0 R_{Ch} + r_{CN} \cdot N_d)(2\Delta x \Delta y H \rho)\} && (3.21)\\
DIC_d^{eq} &\cong pCO_2 \cdot K_0 R_{Cl} \cdot + r_{CN} \cdot N_d \quad LS \ mode && (3.22)\\
pCO_2 &\cong \frac{m^{at}}{M^{at}}\{constant - (pCO_2 \cdot K_0 R_{Cl} + r_{CN} \cdot N_d)(2\Delta x \Delta y H \rho)\} && (3.23)
\end{aligned}
$$

Equation 3.21 is a nonlinear equation of pCO_2 since $K_0 R_{Ch}$ and $K_0 R_{Cl}$ depends on DIC_h and DIC_l. DIC_h and DIC_l in turn depends on pCO_2. By applying $a_0, a_T, a_S, a_{DIC}, T_0, S_0$ and DIC_0 from the Table 2.1, the equation can be solved iteratively. The results for the analytical solution of pCO_2 is 152 ppmv for the HS mode and 504 ppmv for the LS mode. The error for the estimated pCO_2 is larger in the HS mode because the thermohaline intensity is stronger in the HS mode and the approximation tends to overestimate the biological pump with large number for q. Besides calculating the steady state pCO_2, this expression implies several important characteristics of the system.

At the surface ocean,

$$
\begin{aligned}
DIC_0 &= pCO_2 \cdot K_0 R_C(T, S, DIC)\\
&= pCO_2 \cdot (a_0 + a_T \cdot T' + a_S \cdot S' + a_{DIC} \cdot DIC')\\
pCO_2 &= \frac{DIC}{a_0 + a_T \cdot T' + a_S \cdot S' + a_{DIC} \cdot DIC'} \qquad (3.24)
\end{aligned}
$$

where $T' = T - T_0, S' = S - S_0$, and $DIC' = DIC - DIC_0$. The perturbations

terms are relatively small to a_0 and it is possible to rewrite 3.24 as

$$
\begin{aligned}
pCO_2 &= \frac{DIC}{a_0}(1 - \frac{a_T}{a_0}T' - \frac{a_S}{a_0}S' - \frac{a_{DIC}}{a_0}DIC') && (3.25)\\
&= pCO_2{}^0(1 + 0.0472T' - 0.215S' + 0.0052DIC') \quad Alk = Alk(S) && (3.26)\\
&= pCO_2{}^0(1 + 0.0472T' + 0.0175S' + 0.0052DIC') \quad Alk = const && (3.27)
\end{aligned}
$$

First, this relation represents the temperature dependence of the pCO_2. 1°C increase of SST induces 4.72% increase of pCO_2 if the entire ocean is warmed up. This relationship was first suggested as 4.2 % by Eriksson in 1963 (3,10). Bacastow recently estimated this parameter as 4.5% (2). The physical meaning of this relation is the temperature dependence of solubility. The warmer the ocean is, the lower the solubility is, therefore, the ocean has to release pCO_2 into the atmosphere and increases pCO_2.

Second, the relationship reveals the uncertain role of salinity. The relations 3.26 and 3.27 gives totally different perspective of salinity. In the variable alkalinity model, the sign of a_S is positive, whereas in the fixed alkalinity model, it is negative. A simple difference in the parameterization of alkalinity can change the fundamental behavior of the system associated with salinity. In variable alkalinity model, a_S is positive because increasing salinity also means increasing alkalinity. As is explained in the previous chapter, the surface alkalinity may be coupled with SSS since the evaporation and precipitation are the most important processes in controlling the concentration of solute. Increasing alkalinity increases pH, which is a favorable environment for bicarbonate and carbonate species. Therefore increasing salinity reduces pCO_2 at an amazingly large rate. 1 ‰ increase of SSS reduces 21.5 % of pCO_2 at constant temperature and DIC. The ocean maintains relatively moderate salinity gradient in the HS mode and so the SSS effect is not critical in the HS mode. The next section shows that the fixed alkalinity model has very different stationary solution for the LS mode. It suggests that K_0R_C is very sensitive to the parameterization of salinity and alkalinity. Further study could add an alkalinity cycle model to the AOC system,

which is necessary for better understanding the coupling of the dynamics of the AO system and the biogeochemical cycle.

Third, the relation 3.25 implies that the system is nonlinear. In fact, it provides interesting perspective of the buffer or Revelle factor. Suppose $K_0 R_C$ is linear and independent of DIC. At constant temperature and salinity,

$$\begin{aligned} DIC &= pCO_2 \cdot K_0 R_C \\ \delta DIC &= \delta pCO_2 \cdot K_0 R_C \qquad (3.28) \\ \frac{\delta DIC}{DIC} &= \frac{\delta pCO_2}{pCO_2} \qquad (3.29) \end{aligned}$$

The system is too simple to explain the buffer factor. Now we can try the same procedure for the equation 3.25. This time, suppose $K_0 R_C$ is nonlinear and involves DIC.

$$\begin{aligned} DIC &= pCO_2 \cdot K_0 R_C(DIC) \\ \delta DIC &= \delta pCO_2 \cdot K_0 R_C(DIC) + pCO_2 \cdot \delta K_0 R_C(DIC) \\ \delta DIC &= \delta pCO_2 \cdot K_0 R_C(DIC) + pCO_2 \cdot a_{DIC} \delta DIC \\ (1 - pCO_2 \cdot a_{DIC}) \cdot \delta DIC &= \delta pCO_2 \cdot K_0 R_C(DIC) \\ B \cdot \frac{\delta DIC}{DIC} &= \frac{\delta pCO_2}{pCO_2} \qquad (3.30) \end{aligned}$$

With $pCO_2 = 280$ (ppmv), B = 12.6. The buffer factor is typically within the range of 8 to 12. Therefore, the parameterization can also estimate a somewhat acceptable value for the buffer factor. The most important message of this relationship is that the equations of the system must be nonlinear in order to explain the buffer factor. This is why the nonlinear carbon chemistry equation is normally solved iteratively. The physical explanation of this nonlinearity is quite simple. The more DIC the ocean contains, the lower the pH is. Because DIC is mainly in the form of bicarbonates and carbonates, the capacity of the ocean as a reservior of DIC rapidly shrinks when pH

goes too low. The relation 3.26 and 3.27 implies that a 1 $\mu mol/kg$ increase of DIC increases $K_0 R_C$ by 0.52 % at constant temperature and salinity. Therefore, increasing DIC raises pCO_2 more rapidly than a simple linear increase. A small change in DIC can induce a large change in pCO_2, whose ratio is about ten, the buffer factor.

In summary, the steady state pCO_2 is determined by the SSS, SST and the sign of q through following procedure. The sign of q determines the outcropping ocean. If q is positive, the high latitude ocean determines the property of the deep ocean. If q is negative, the low latitude ocean is the outcropping ocean. Since the deep ocean is by far the largest reservoir of DIC, pCO_2 is determined by the property of the deep ocean. SST and SSS determines the property of the outcropping ocean. In the LS mode, pCO_2 is very high because the outcropping ocean is at low latitudes. The tropical temperature made the solubility so low that the solubility pump became very inefficient.

3.4 The fixed Alkalinity model

The models which has been discussed so far assumed that the alkalinity can be approximated as a linear function of SSS. Another set of models can be created with a fixed total alkalinity. The most simple model is the fixed alkalinity model which can be easily derived from the original AOC model. The fixed alkalinity condition requires $K_0 R_C(T, S, DIC)$ to be re-calculated without the relation 2.82. Table 2.2 shows the parameters calcualted based on $Alk = 2317(\mu eq \cdot kg^{-1})$. The entire experiment can be repeated with this set of parameters although this study only includes a few important results.

The workstation could only calculate the HS steady state for the fully-coupled fixed alkalinity model. The LS solutions requires very small time step and it exceeded the capacity of available computational resources to integrate long enough that the system reaches its steady state. Table 3.5 shows the direct output from the model runs. Compared to the former model runs, most of the parameters remains unchanged except for pCO_2 and DIC. In fixed alkalinity model, the HS mode has similar pCO_2

and DIC. But the LS mode has totally different distribution of DIC, and its pCO_2 exceeds 1000 ppmv and still increasing after 5000 years of integration. The global warming feedback is accelerating the increase of pCO_2. The simple difference in the assumption on alkalinity can totally change the steady solution of the system in the LS mode.

Salinity plays an important role in the LS, salinity-driven, mode. The SSS gradient is much larger in the LS mode than in the HS mode. The sea water sinks at low latitudes because the high salinity outweighs the thermal expansion. This high salinity is connected to high alkalinity in the standard, variable alkalinity model. When 2.82 is applied to estimate alkalinity in the variable alkalinity model, its alkalinity is higher than the fixed alkalinity model. According to the charge balance equation 2.78, the more alkalinity the ocean has, the more DIC can be stored in the ocean. In the Table 2.1 and 2.2, the parameter a_S is positive in the various alkalinity model and is negative in the fixed alkalinity model. That means that $K_0 R_C$ increases by a_S when one more unit of salinity is added to the system. Given a fixed DIC concentration, the larger $K_0 R_C$, the less pCO_2 is expected in steady states. Consequently, pCO_2 decreases with increasing SSS in the variable alkalinity models, whereas pCO_2 increases in the fixed alkalinity models. The LS solution of the variable alkalinity models had relatively lower pCO_2 because the high salinity at low latitudes suppressed the increase of pCO_2 by increasing the alkalinity.

As one can see, the difference in the expression of alkalinity changed a fundamental behavior of the model. The increase in SSS enhances the capacity of the ocean as a reservoir of DIC in the variable alkalinity model because an increase in SSS means an increase in alkalinity as well. On the other hand, the opposite is true in the fixed alkalinity model. The main results of this study is based on the variable alkalinity model.

Table 3.1: Model parameters for the AOC model

Simbol	Value	Definition
h_{AO}	500	Thickness of Mixed layer(m)
H	5000	Depth of the ocean(m)
ρ	$1.035 \cdot 10^3$	Density of the sea water(kgm^{-3})
ρ_C	$4.0 \cdot 10^6$	Heat capacity of the sea water($Jm^{-3}K^{-1}$)
A_{h0}	$-1.23 \cdot 10^9$	Radiation constant at high lat.($J \cdot yr^{-1}m^{-2}$)
A_{l0}	$2.87 \cdot 10^9$	Radiation constant at low lat.($J \cdot yr^{-1}m^{-2}$)
A_{h1}	$1.58 \cdot 10^8$	Radiation-pCO_2 coeff. at high lat.($J \cdot yr^{-1}m^{-2}$)
A_{l1}	$2.78 \cdot 10^8$	Radiation-pCO_2 coeff. at low lat.($J \cdot yr^{-1}m^{-2}$)
B	$5.36 \cdot 10^8$	Long-wave radiation constant($J \cdot yr^{-1}m^{-2}$)
χ	$4.10 \cdot 10^7$	Atmos. heat transport coeff.
γ	$8.82 \cdot 10^{-3}$	Atmos. moisture transport coeff.
ε	0.5	
ε_W	0.5	
α	$1.8 \cdot 10^{-4}$	Thermal expansion coeff.
β	$0.8 \cdot 10^{-3}$	Saline expansion coeff.
k	0.63	Thermohaline coeff.(yr^{-1})
h_C	100	Thickness of euphotic layer(m)
λ_h	0.5	Biological productivity at high lat.(yr^{-1})
λ_l	2.5	Biological productivity at low lat.(yr^{-1})
r_{CN}	106/16	Redfield ratio of carbon to nitrate
μ	1	Air-sea DIC exchange coeff.(yr^{-1})
m	0.0288	Molecular mass of the air($kg \cdot mol^{-1}$)
M^{at}	$5.14 \cdot 10^{18}$	Mass of the entire air(kg)
Δx	$18 \cdot 10^6$	Longtudional extent of the box(m)
Δy	$10 \cdot 10^6$	Latitudional extent of the box(m)

Figure 3-1: The structure of the AOC system

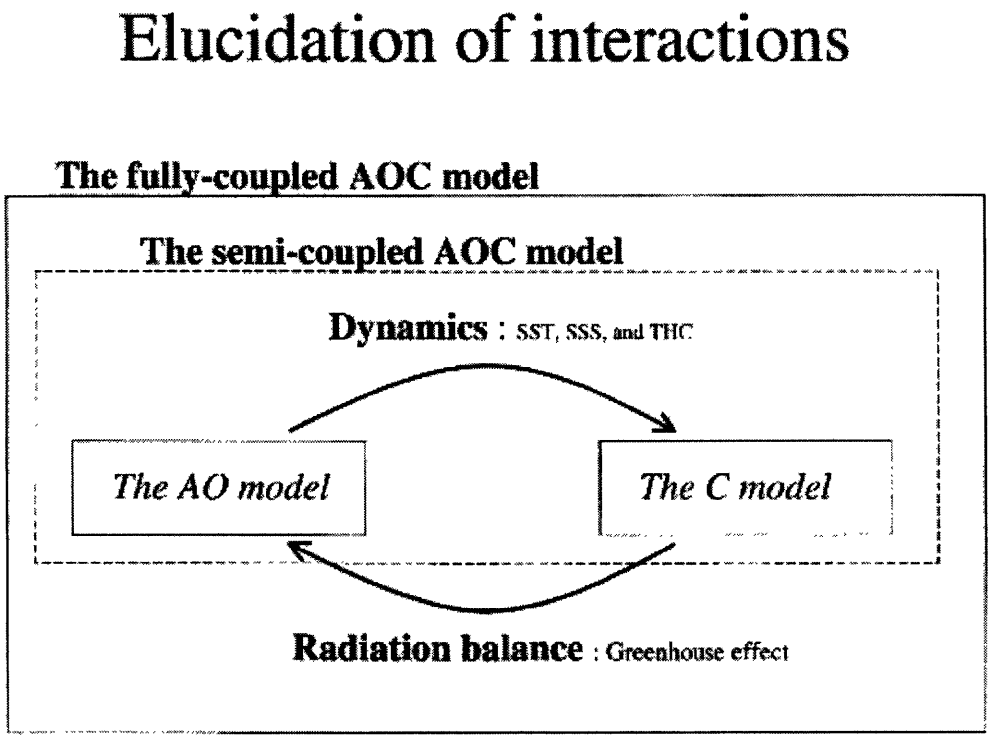

Figure 3-2: The system behavior of the AOC model

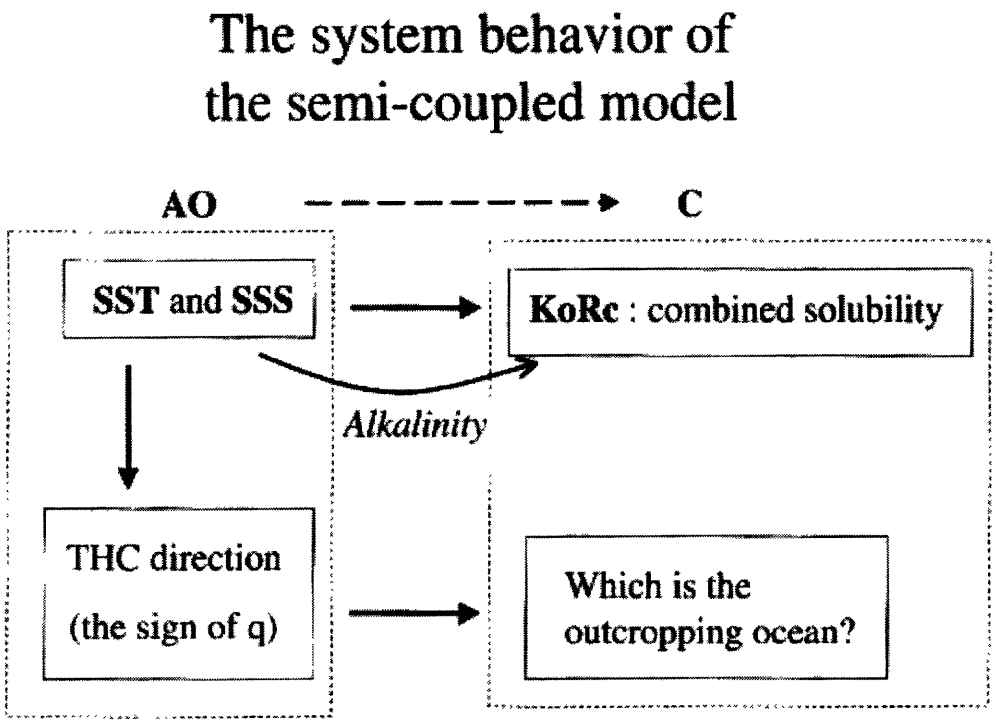

Figure 3-3: The competing effect between the outgassing and the biological pump

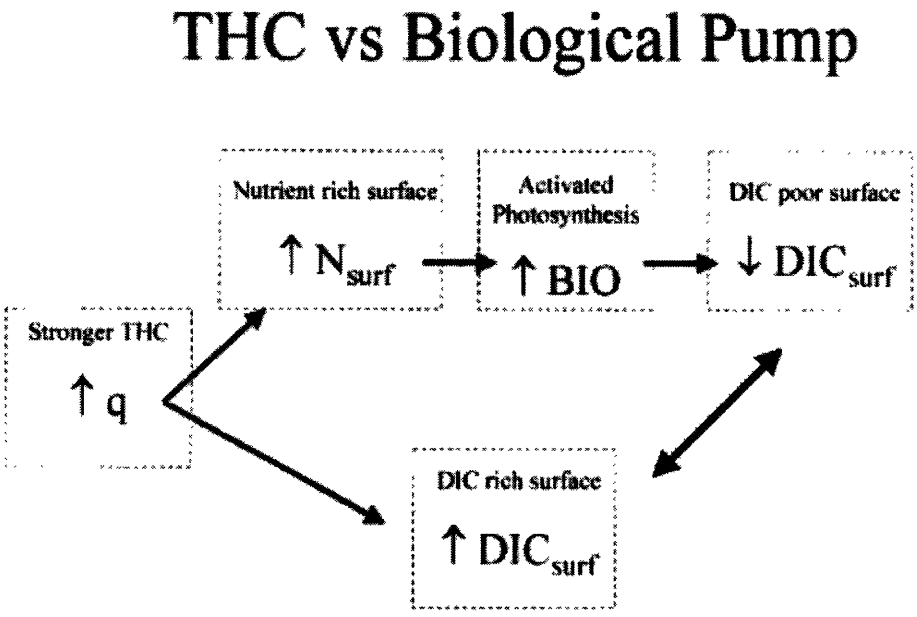

Figure 3-4: The effect of $\mid q \mid$ on pCO_2

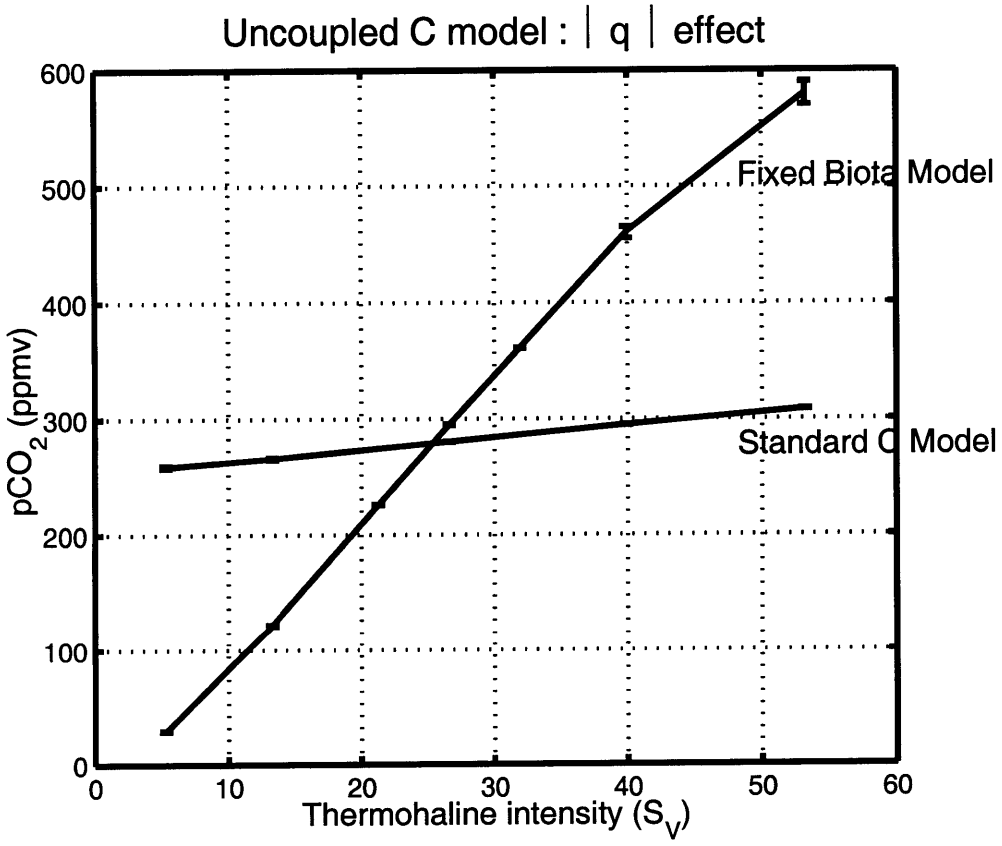

Table 3.2: Initial conditions for the fully coupled AOC model

Parameters	HS	LS	Unit
N_h	5	5	μM
N_l	0.5	0.5	μM
N_d	30	30	μM
DIC_h	2180	2180	μM
DIC_l	2090	2090	μM
DIC_d	2360	2360	μM
pCO_2	360	360	ppmv
T_h	5	5	C
T_l	25	25	C
T_d	15	15	C
S_h	34	31	$\%_0$
S_l	36	39	$\%_0$
S_d	35	35	$\%_0$

Table 3.3: Steady states of the fully coupled AOC model

Parameters	HS	LS	Unit
N_h	2.6	0.7	μM
N_l	0.6	0.6	μM
N_d	30	30	μM
DIC_h	2183	2012	μM
DIC_l	2045	2157	μM
DIC_d	2365	2352	μM
pCO_2	261	537	ppmv
T_h	2.5	2.8	C
T_l	26.0	31.4	C
T_d	2.5	31.4	C
S_h	34.9	29.3	$‰$
S_l	36.5	36.7	$‰$
S_d	34.9	35.2	$‰$
THC	26.6	-6.95	S_V
T_M	14.3	17.1	C
BIO_h	0.880	0.238	$molC \cdot m^{-2} \cdot yr^{-1}$
BIO_l	0.952	1.014	$molC \cdot m^{-2} \cdot yr^{-1}$
Int.H.Trans.	1.32	-0.380	$GTC \cdot yr^{-1}$

Table 3.4: Steady states of the semi-coupled AOC model

Parameters	HS	LS	Unit
N_h	2.6	0.7	μM
N_l	0.6	0.6	μM
N_d	30	30	μM
DIC_h	2182	2026	μM
DIC_l	2055	2159	μM
DIC_d	2364	2354	μM
pCO_2	280	496	ppmv
T_h	3.5	1.1	C
T_l	27.1	29.4	C
T_d	3.5	29.4	C
S_h	34.9	29.3	$‰$
S_l	36.5	36.6	$‰$
S_d	34.9	35.2	$‰$
THC	26.7	-6.71	S_V
T_M	15.3	15.3	C
BIO_h	0.88	0.24	$molC \cdot m^{-2} \cdot yr^{-1}$
BIO_l	0.95	1.01	$molC \cdot m^{-2} \cdot yr^{-1}$
Int.H.Trans.	1.32	-0.38	$GTC \cdot yr^{-1}$

Table 3.5: Model output from the fixed alkalinity model runs

Parameters	HS(steady)	LS(at 1000 yr)	Unit
N_h	2.6	0.7	μM
N_l	0.6	0.6	μM
N_d	30	30	μM
DIC_h	2183	2263	μM
DIC_l	1991	2129	μM
DIC_d	2365	2327	μM
pCO_2	271	1003	ppmv
T_h	2.6	5.0	C
T_l	26.1	34.0	C
T_d	2.6	33.3	C
S_h	34.9	29.2	$\%_0$
S_l	36.5	36.7	$\%_0$
S_d	34.9	35.2	$\%_0$
THC	26.6	-6.71	S_V
T_M	14.4	19.5	C
BIO_h	0.88	0.24	$molC \cdot m^{-2} \cdot yr^{-1}$
BIO_l	0.95	1.01	$molC \cdot m^{-2} \cdot yr^{-1}$
Int.H.Trans.	2.04	-0.41	$GTC \cdot yr^{-1}$

Chapter 4

Feedback mechanism

4.1 Global warming feedback

The global warming feedback is the primary feedback mechanism in the AOC system although it is quite simple. First, assume a perturbation in pCO_2 with some increment. The increased pCO_2 raises the global mean temperature by greenhouse effect. Solubility decreases as the ocean warms up, and it releases CO_2 into the atmosphere to compensate the decreasing capacity of CO_2 in the ocean. This effect further enhances the initial perturbation of the incremental pCO_2. This positive feedback does not explicitly involve thermohaline circulation.

The previous chapter showed some numerical experiments about the comparison of the fully-coupled model and the semi-coupled model in section 3.2. In the fully-coupled model, the global warming feedback, the global mean temperature (T_M) decreased by 1°C and pCO_2 also decreased by 19 ppmv in the HS mode. T_M increased by 1.8°C and pCO_2 increased by 41 ppmv in the LS mode. From these results, 1°C increase of T_M is associated with pCO_2 increase of about 20 ppmv. Eriksson (10) estimated the effect of the ocean warming on pCO_2 in 1963 and showed that 1°C increase in T_M increases pCO_2 by 4.2 %. The C model estimated about 4.5 % increase through the parameterization of $K_0 R_C$. Then, the effect of ocean warming alone can raise pCO_2 by 13 ± 1 ppmv, which is significantly smaller than 20 ppmv. Therefore, the global warming feedback actually enhanced the response of the ocean

to the global warming.

4.2 Thermohaline pCO_2 feedback

4.2.1 Clausius-Clapeyron relationship

Several feedback mechanism can be introduced when the Clausius-Clapeyron (CC) relationship is added to the AOC system. The intensity of the thermohaline circulation solely depends on the SST and SSS gradient between high and low latitudes and does not explicitly depend on the global mean temperature without the CC relationship. Carbon cycle could perturb T_M significantly but could not affect the SST or SSS gradient. It is the primary reason the C part of the model mostly played a passive role in the AOC climate system. However, the recent GCM experiment by Manabe et al (18) showed that increasing pCO_2 could weaken or even halt the thermohaline circulation. The weakening of thermohaline circulation is based on the increased salinity gradient due to the increased atmospheric moisture transport. The CC relationship describes the relationship between temperature and the saturation vapor pressure, and it connects T_M and the atmospheric moisture transport in the context of this study. It approximated the atmospheric moisture transport as a linear function of latitudinal temperature gradient but it is possible to modify the parameterization with CC relationship.

$$F_m \rightarrow F_m \cdot (\frac{273 + T_{ME}}{273 + T_M}) \cdot \exp\{-5420(\frac{1}{273 + T_M} - \frac{1}{273 + T_{ME}})\} \qquad (4.1)$$

T_{ME} is the standard mean temperature. In this study, T_{ME} is set to 15.3° C. As T_M becomes higher, the atmospheric moisture transport increases also. Figure 4-2 is the schematic diagram for the effect of CC relationship on the thermohaline circulation and Figure 4-3 plots the factor of the enhanced moisture transport due to the changes in global mean temperature. The moisture transport responds to the rising temperature roughly linearly. The increased moisture transport then increases the latitudinal salinity gradient. The higher the T_M is, the weaker the thermohaline

circulation is in the HS mode. This relationship connects the global mean temperature to the latitudinal salinity gradient and thermohaline intensity. As it is discussed in the previous chapter, changes in thermohaline intensity could induce several patterns of potential perturbation on pCO_2.

4.2.2 $\mid q \mid$ and pCO_2

When the CC relationship is added to the AOC model, the global warming can weaken the intensity of thermohaline circulation. Then, the weakened thermohaline circulation could perturb the carbon cycle and it may cause positive or negative feedbacks. If the weakening of the thermohaline circulation causes further increase in pCO_2, it establishes a positive feedback. If the weakening of thermohaline circulation causes a reduction of pCO_2, it then establishes a negative feedback. In this study, those feedbacks are collectively called the thermohaline pCO_2 feedback. The previous chapter introduced some important processes which may affect the relationship between $\mid q \mid$ and pCO_2. The combination of Figure 3-3 and 4-2 gives the picture of the possible thermohaline pCO_2 feedbacks.

First, weakening of the thermohaline circulation makes the biological pump very inefficient by limiting the supply of nutrients at low latitudes. If the vertical mixing is also coupled to the density structure of the ocean, the biological pump at high latitudes is also weakened. The process results in an increase in pCO_2, which means positive feedback.

Second, the weakening of the thermoahline circulation reduces the outgassing rate at low latitudes. The upwelling of deep water at warm, low latitudes, surface ocean releases excess CO_2 into the atmosphere. The outgassing rate is correlated to the intensity of the thermohaline circulation. Intensifying the thermohaline circulation results in an increase in pCO_2, therefore, the weakening of the thermohaline circulation cools down the global mean temperature. The weakening of the thermohaline intensity caused by the global warming will be moderated by the reduction of pCO_2 to some extent. The process establishes a negative feedback, which tends to compensate the positive feedback described previously. The compensation of the outgassing effect

and the biological pump is based on the discussion in the previous chapter. Figure 4-4 shows the competing effect between the outgassing effect and the biological effect based on stationary states of the uncoupled C model.

Finally, there is a DIC exporting feedback. This feedback mechanism only applies to the transient states which is similar to the anthropogenic global warming. When an external source rapidly increases atmospheric CO_2, the excess CO_2 slowly invades the ocean. If the system were in equilibrium, the ocean can uptake about 90 % of CO_2 emission according to Bolin and Eriksson (3). Although the ocean has a huge capacity for carbon in equilibrium, the ocean currently uptakes only < 25 % of CO_2 emission. Equation 2.70 shows that the surface mixed layer can be equilibrated with the atmospheric CO_2 around the order of 10^0 year. It takes a long time for CO_2 to equilibrate with the deep ocean because the time scale for mixing the deep ocean is around the order of 10^3 years. The mixing time scale for the deep ocean depends on the thermohaline intensity. Therefore, weakening of the thermohaline circulation slows down the rate of exporting DIC to the deep ocean and results in less oceanic uptake of CO_2. Therefore, it establishes a positive feedback. This feedback is called DIC exporting feedback. Figure 4-5 summarizes the schematic diagram for the global warming feedback and the thermohaline pCO_2 feedback.

From the Newtonian dumping point of view, the positive and the negative feedback have exactly the same time scale because they are both controlled by the perturbation of thermohaline circulation induced by the CC relationship. The adjustment time scale for the thermohaline circulation is several hundred years. On the other hand, the time scale of the global warming feedback is quite short because the radiation balance adjusts much faster than ocean circulation. The coupling of physics and chemistry of the AOC system involves a wide range of time scale. The carbon chemistry reacts very fast compared to the general circulation of atmosphere-ocean coupled system, but the carbon chemistry is largely affected by SSS, SST and the thermohaline circulation.

4.3 Global warming simulation

4.3.1 Setting up the experiment

The AOC model with the CC relationship can explore an idealized simulation of the global warming. It explains several aspects of the recent GCM global warming simulations done by Manabe et al (18), and Sarmiento et al (25). The strength of the AOC model is that it does not need to prescribe the time evolution of atmospheric pCO_2. The C model is able to calculate both DIC and pCO_2 based on the total amount of carbon in the system. Therefore, it is possible for the AOC model to simulate global warming without making assumptions on pCO_2. It also allows the feedback mechanisms between pCO_2, T_M, $\mid q \mid$, or other parameters within the system.

According to Siegenthaler and Sarmiento (27), the CO_2 emission due to human activities is pumping carbon into the atmosphere by 7 GTC every year, out of which 5 GTC is from the fossil fuel burning and 2 GTC is from the deforestation. About 30 % of the emission goes into the ocean and 45 % remains in the atmosphere. Therefore, there is about 25% net imbalance between the emission and the sink. The missing sink might be in the terrestrial biosphere.

The simple global warming simulation was done in the following procedure. The spin up of the model first calculates the steady state solution of the HS mode. It takes about 5000 years to reach the equilibrium. Then, the model starts to add to the atmosphere 7 GTC of carbon every year. The model does not have any constraint on pCO_2 nor DIC so that the perturbed pCO_2 freely invades the ocean. Some portion of the 7 $GTC \cdot yr^{-1}$ emission goes into the ocean and other portion remains in the atmosphere.

Figure 4-6 and 4-7 are the time evolution of the atmospheric pCO_2 and the thermohaline intensity of various model runs. As pCO_2 increases, the thermohaline intensity decreases because of the stimulated atmospheric moisture transport by the CC relationship. The rate of increase in the atmospheric CO_2 indicates that the 86 % of CO_2 emission remains in the atmosphere in the fully coupled model. pCO_2 increased about 1700 ppmv during 600 years of the emission.

$$\begin{aligned}
\Delta C_{atm} &\approx 1700(ppmv) \cdot \frac{M^{at}(kg)}{m^{at}(kg \cdot mol)} \\
&= 1700 \cdot 10^{-6} \cdot \frac{5.14 \cdot 10^{18}}{0.0288}(mol) \\
&= 30.3 \cdot 10^{16}(molC) \\
&= 3630(GTC) \qquad (4.2)
\end{aligned}$$

Over the 600 years, the atmosphere received $7(GTC \cdot yr^{-1}) \cdot 600(years) = 4200(GTC)$ of carbon, out of which 3630 (GTC) remained within the atmosphere. It indicates that 14 % of CO_2 are uptaken by the ocean, which is in the same order with the previous work (27) but it is still significantly smaller than the accepted value of 25 %. A set of similar experiment was repeated with less emission of 1.92 GTC yr^{-1}. Then, pCO_2 increased by 340 (ppmv) for 500 years, which indicates that the oceanic uptake was 24.2 % in this case. Therefore, the rate of oceanic uptake depends on how fast the global warming proceeds. The thermohaline circulation was significantly weakened by increasing pCO_2. The next section examines the effect of global warming on the stability of the thermohaline circulation.

The fixed Biota model keeps nitrate constant in the AOC system, therefore it cuts off the biological pump feedback. The weakening of the thermohaline circulation does not decrease the biological export production. This model has slower pCO_2 increase rate because the fixed Biota model is more stable than the fully coupled model. Uncoupled C model does not have any feedback mechanism and is the most stable model among the three model runs. Therefore, one can conclude that the four feedback mechanisms have net positive feedback effect to the system.

4.3.2 Stability analysis

Further emission of CO_2 results in the spontaneous transition to the LS mode at around 2000 ppmv for pCO_2 and it takes about 550 years of the emission time span with the rate of $7GTC \cdot yr^{-1}$. The GCM experiment by Manabe et al (18) showed that

just quadrupling pCO_2 can induce such transition to another equilibrium state. The AOC model might be underestimating the effect of the weakening of the themohaline intensity although the difference is within the same order of magnitude. The stability analysis of the system actually shows that the global warming destabilize the system before the system reaches the spontaneous transition. Even more interestingly, the feedback mechanism described in the previous section affects the stability of the system.

The stability of the AOC system can be measured by some characteristic parameters. There is not a single parameter which can perfectly express the stability of the AOC system but there are a few important benchmarks developed previously (21). S_{crit} is defined to be the critical salinity perturbation which can cause the transition to the LS mode. The larger the S_{crit} is, the more stable the system is. Another benchmark is the restoration time scale for a weak salinity perturbation. When a weak perturbation are given to the AOC system, the thermohaline intensity is once weakened but it recovers the original strength after a period of time. The decay time $\tau_{\frac{1}{2}}$ was defined as the half life of the perturbation on the thermohaline intensity. The longer the restoration time is, the less stable the systems is. In this study, the weak perturbation was chosen to be $\Delta S = 1.0(\%_0)$. These two stability parameters are measured every 50 years in the global warming simulation with 7 $GTC \cdot yr^{-1}$ and are also measured every 300 years in the global warming simulation with 1.92 $GTC \cdot yr^{-1}$.

Figure 4-8 shows the plot of S_{crit} versus the length of the period of CO_2 emission. The S_{crit} decreases roughly linearly as the emission time span increases. The error bar stands for the uncertainty in measuring the critical perturbation. Several hundreds years of 7 $GTC \cdot yr^{-1}$ emission can decrease S_{crit} more than 50 %.

Figure 4-9 shows the time evolution of the thermohaline intensity after the weak perturbation of $\Delta S = 1.0(\%_0)$. The thermohaline intensity recovers in different time scales depending on the stability of the system. It does not quite follow the Newtonian dumping rule. Figure 4-10 is the plot of the half life, $\tau_{\frac{1}{2}}$, versus the length of the time period of the emission. The restoration time increased as the emission time span increased but it is not a linear relationship.

A similar experiment was repeated with the constant Biota model. The model fixed the concentration of nutrients for each box of the ocean so that the biological pump is not affected by the thermohaline intensity. It cuts off the effect of the thermohaline pCO_2 positive feedback introduced in the previous section. Figure 4-11 compares the S_{crit} of the standard model and that of constant Biota model. The dashed line is the least square trend line for the stability of the models. The constant Biota model is slightly more stable than the standard model. This stability analysis showed that the constant Biota model suppresses the positive feedback and stabilizes the thermohaline intensity but the effect is quite small. The reason the thermohaline pCO_2 feedback is so weak is that it acts only through the coupling of the radiation balance and the CC relationship. The response of radiation balance to the pCO_2 is logarithmic, which implies that pCO_2 has to increase exponentially in order to induce a linear increase of T_M. Moreover, the CC relationship relates T_M and the atmospheric moisture transport roughly linearly, but the magnitude of the effect is relatively moderate.

In summary, the simulation showed that the global warming due to the human activity can reduce the stability of the thermohaline circulation. The model estimated that it takes less than 700 years for the current emission rate to halt the thermohaline circulation. This estimate is still quite larger than the Manabe's result, but this AOC model still overestimates the pCO_2 increase because it ignores the existence of the missing sink. The stability of the system, on the other hand, significantly decreased long before it reaches the transition to the LS mode. Therefore, I conclude that the AOC model with CC relationship can produce a simple representation of the hypothesis of the possible shutdown of the thermohaline circulation by the global warming.

Figure 4-1: A schematic diagram for the global warming feedback

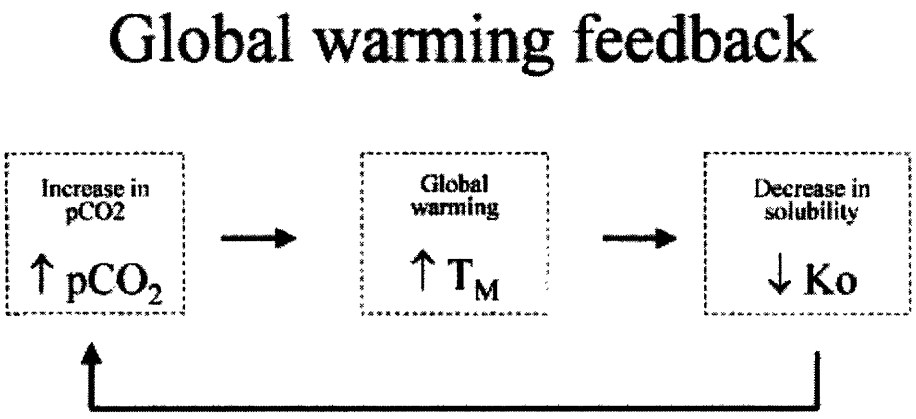

Figure 4-2: A schematic diagram for the effect of Clausius-Clapeyron relationship

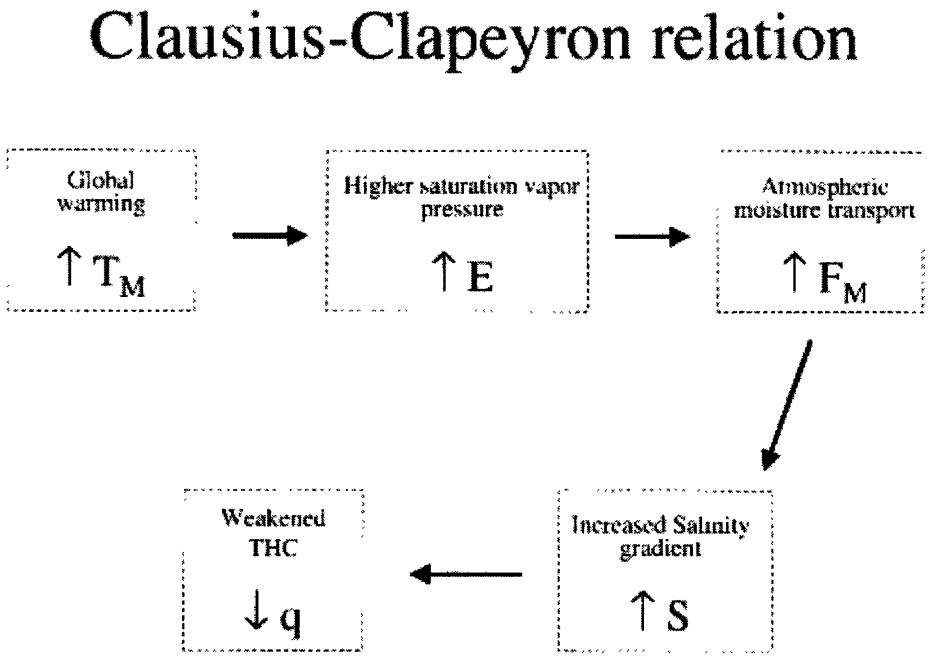

Figure 4-3: The response of atmospheric moisture transport to the global warming

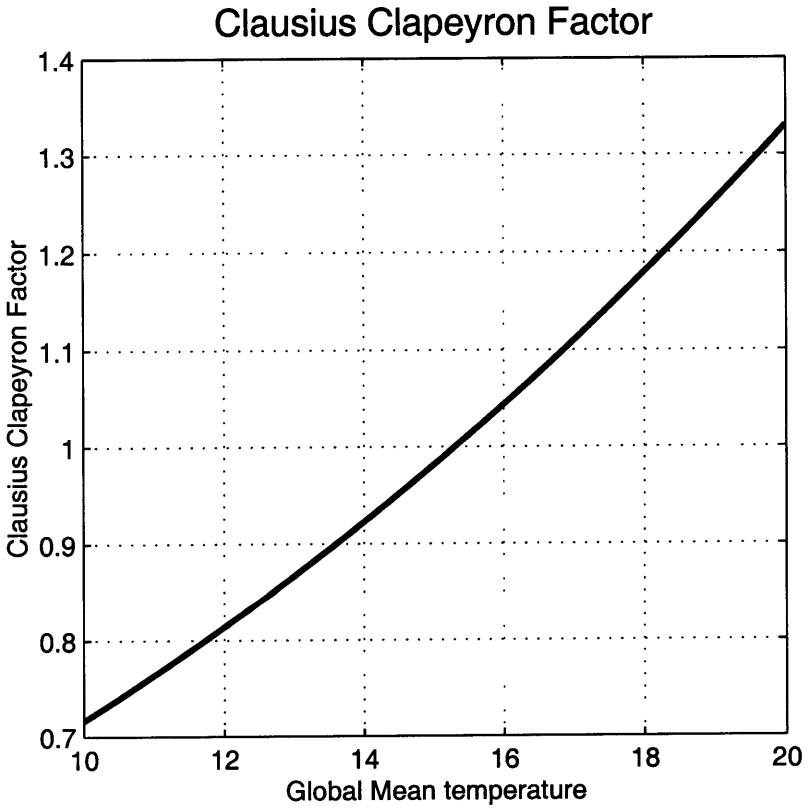

Figure 4-4: The relationship between pCO_2 and $\mid q \mid$ under different assumption

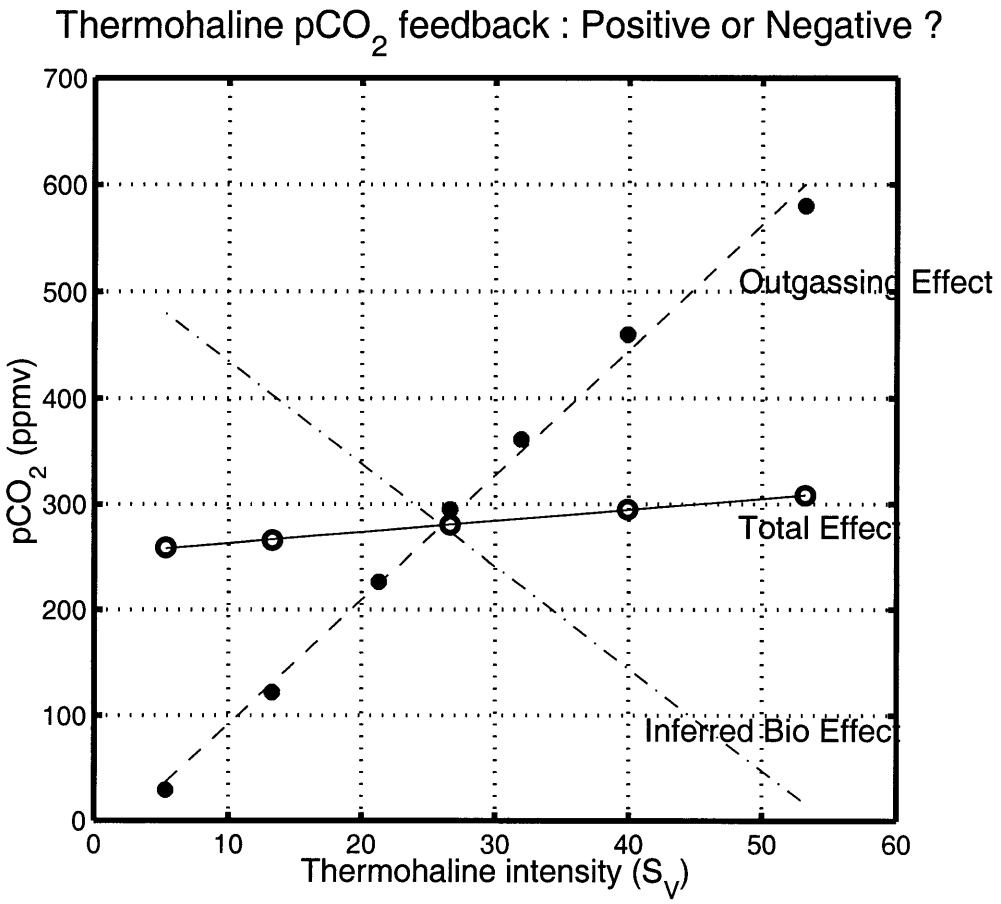

Figure 4-5: The feedback mechanisms

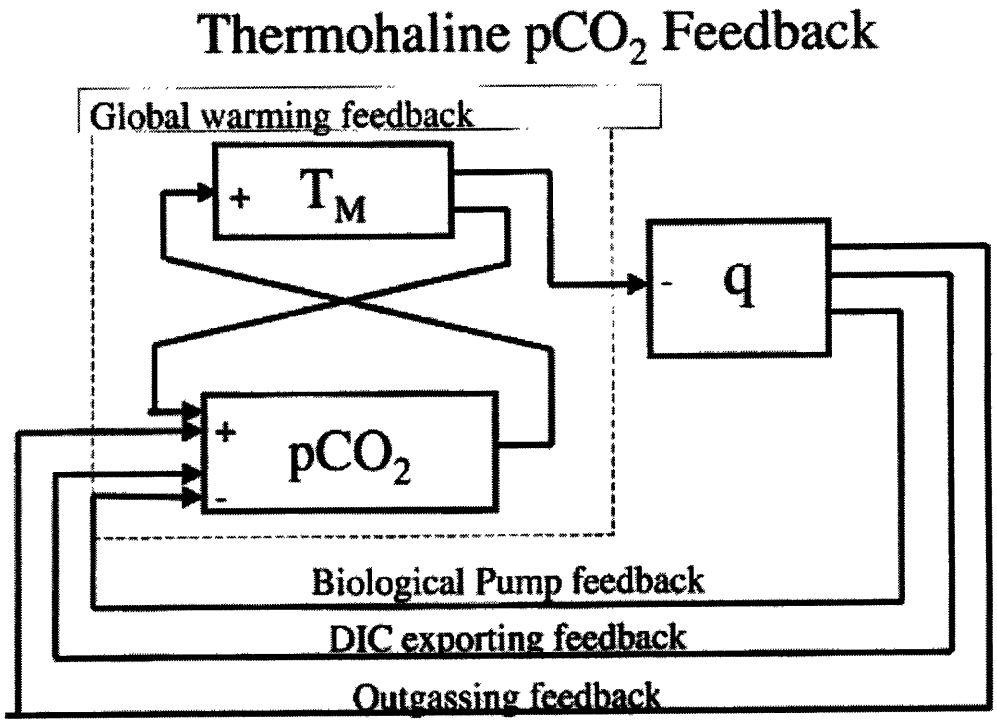

Figure 4-6: The time evolution of pCO_2 in the global warming simulation

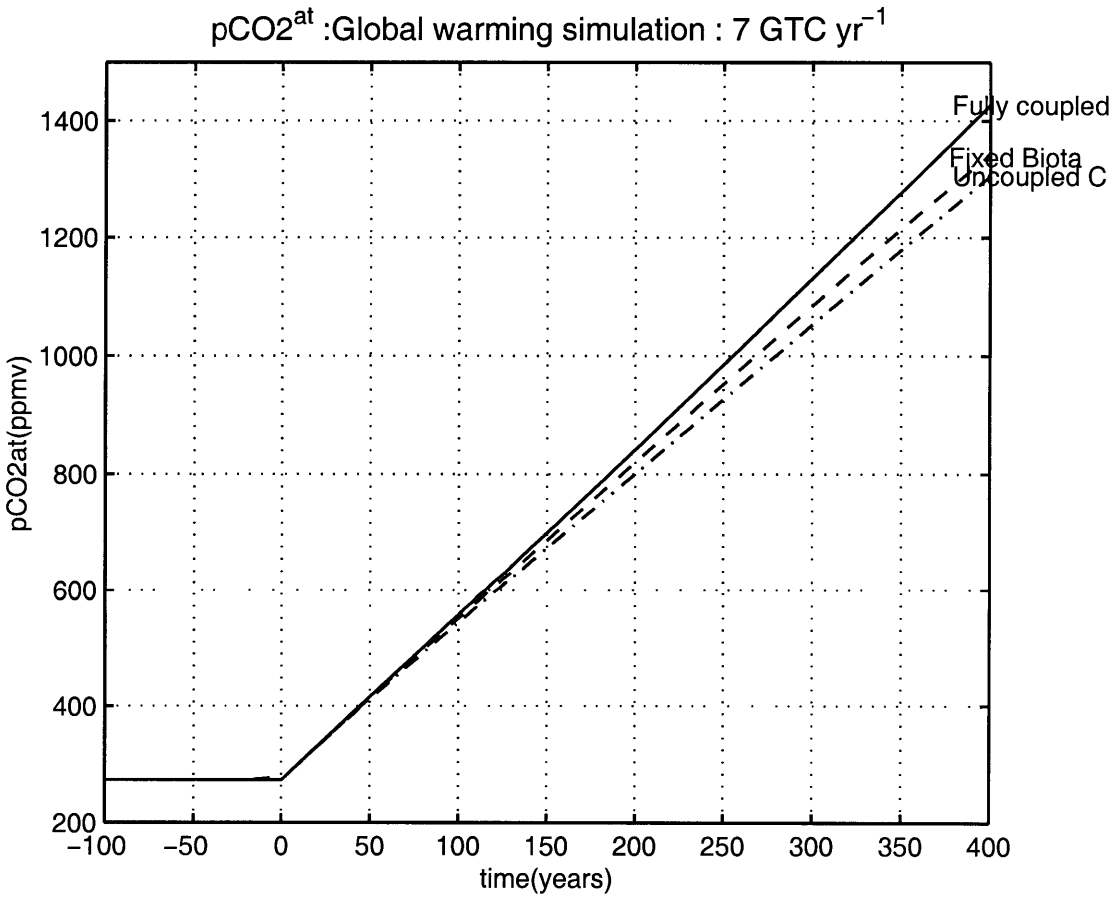

Figure 4-7: The time evolution of $\mid q \mid$ in the global warming simulation

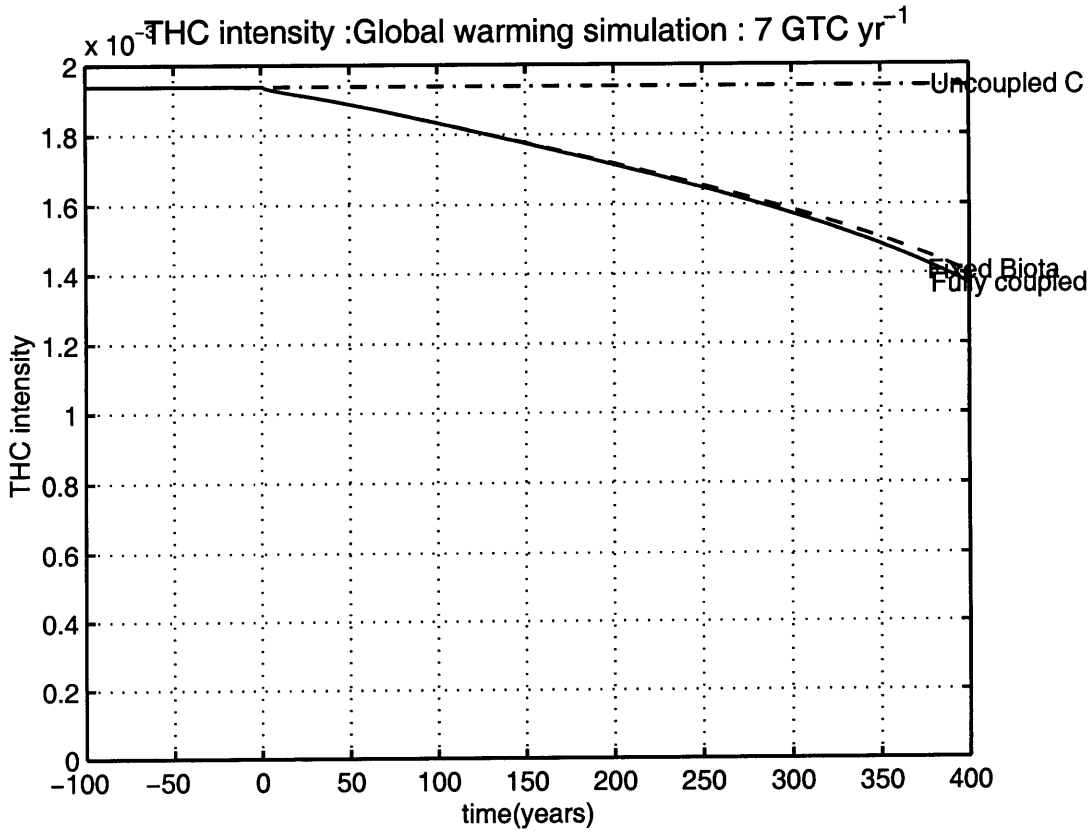

Figure 4-8: S_{crit} versus the emission time span

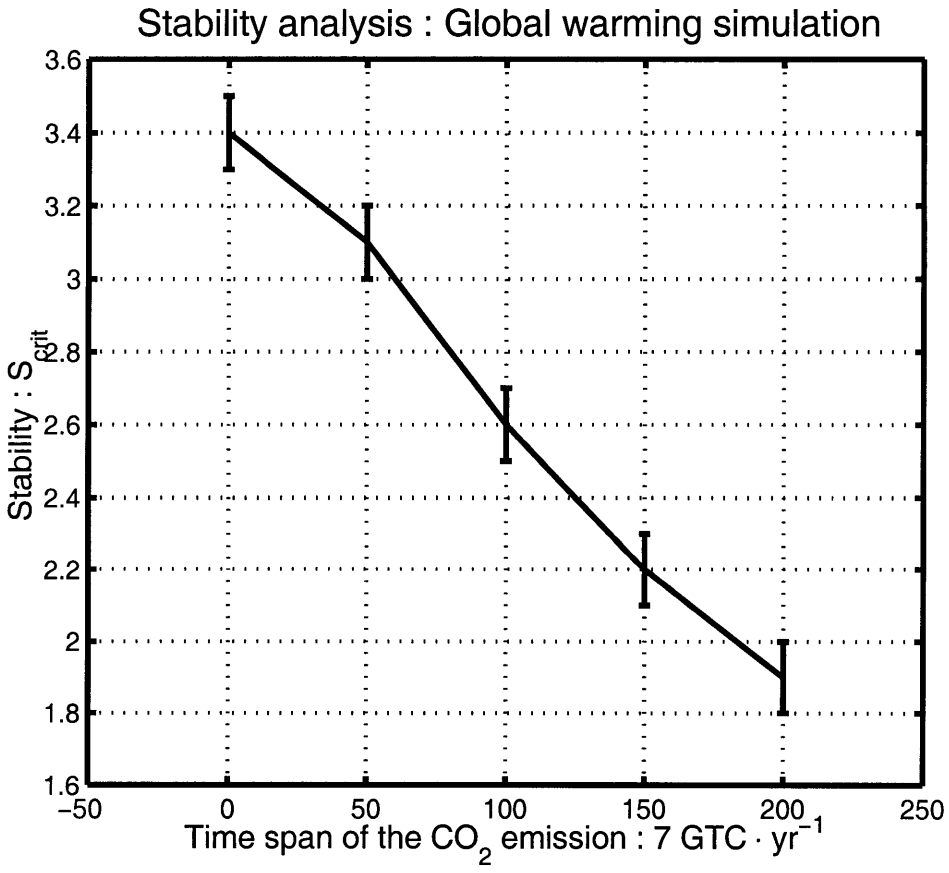

Figure 4-9: The restoration of the thermohaline intensity

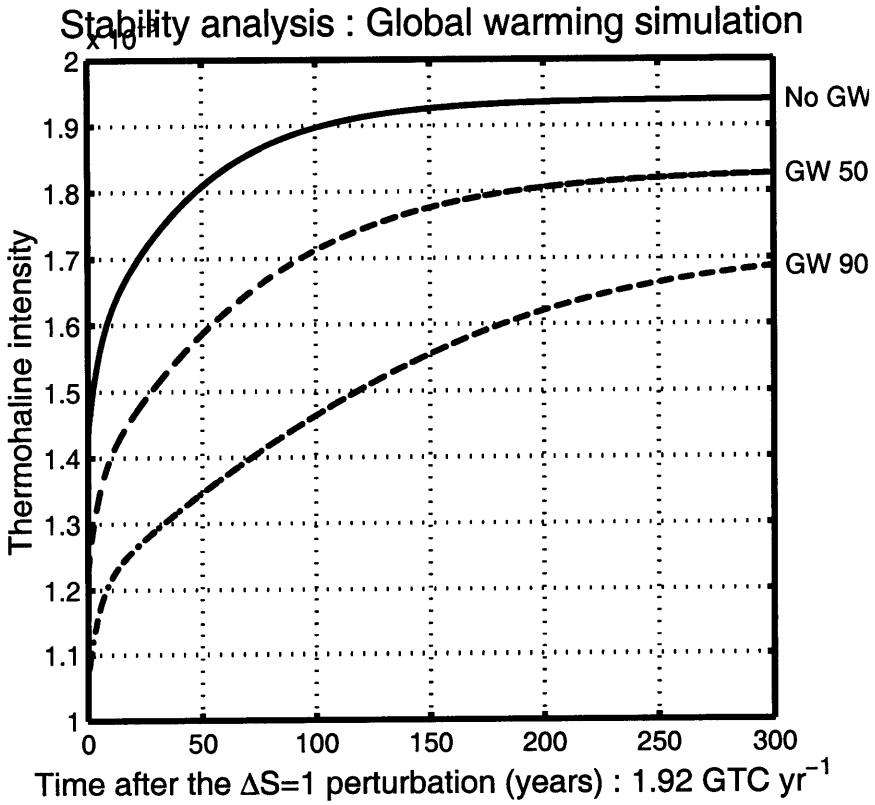

Figure 4-10: The restoration time scale versus the emission time span

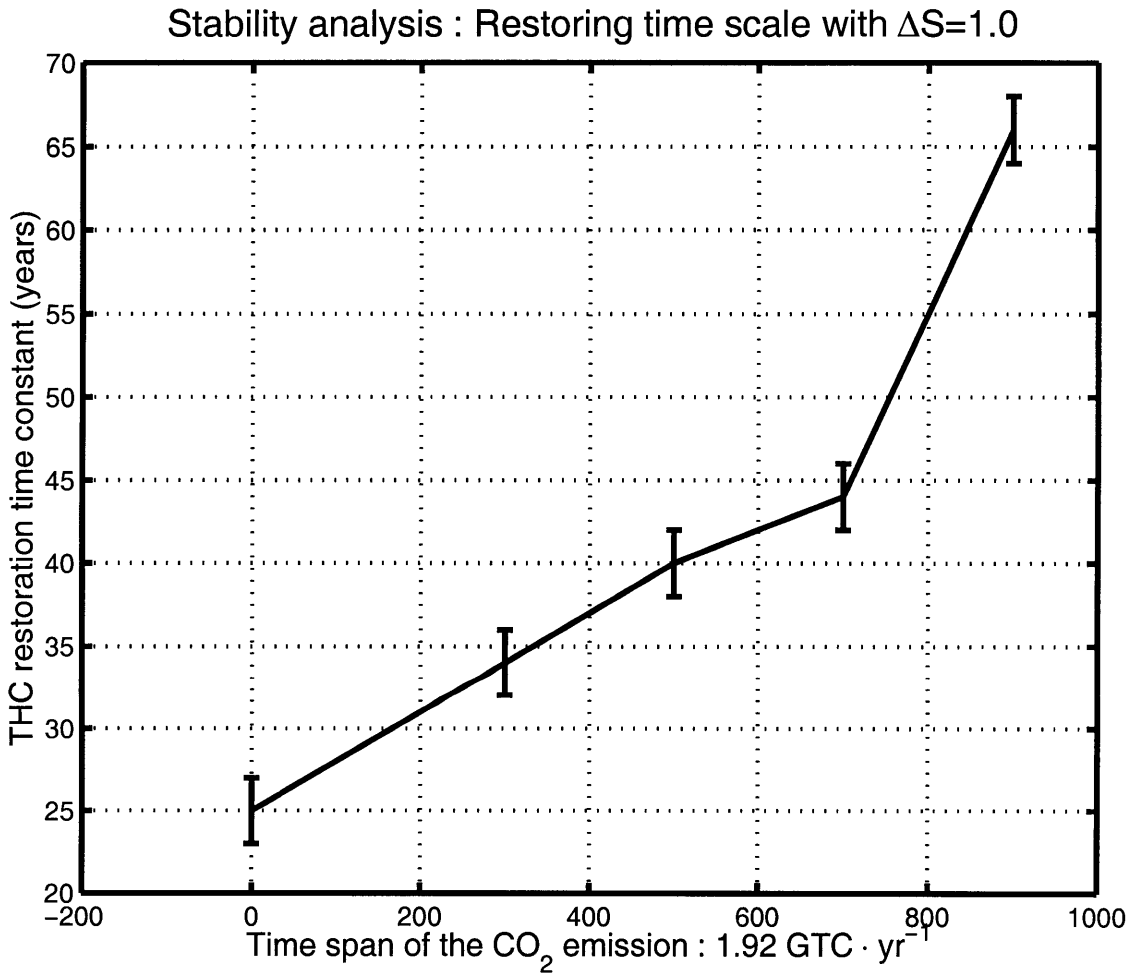

Figure 4-11: The comparison of the S_{crit} : Thermohaline pCO_2 feedback

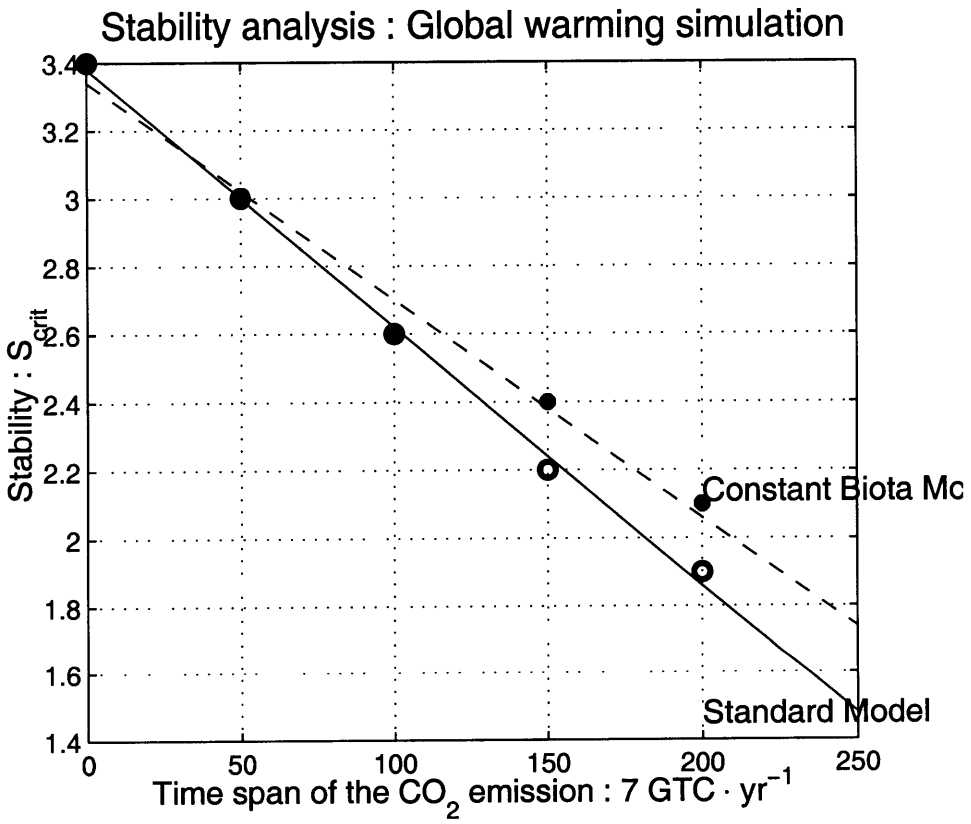

Chapter 5

Discussion and Conclusion

5.1 Summary

This study introduced a fully interactive atmosphere-ocean-carbon (AOC) coupled box model, which elucidated the interaction and the feedback mechanisms between the atmosphere-ocean (AO) system (20,21) and the carbon cycle (C) system (Follows). It introduced a parameterization of the oceanic carbon chemistry rather than solving the full carbon equation iteratively. With the new paremterization, the AOC model could efficiently step forward and solve the twelve ODEs 2.27 $\sim$ 2.38, 2.39 $\sim$ 2.44, and 2.87 $\sim$ 2.92.

The AOC coupled system has two steady states, which are the thermally-driven high latitude sinking (HS) mode and the salinity-driven low latitude sinking (LS) mode. The LS mode had considerably higher atmospheric pCO_2 than the HS mode. Uncoupled C model explained the reason the HS mode and LS mode has different pCO_2 at steady states. pCO_2 mainly depends on the deep ocean DIC concentration and the deep ocean DIC also depends on the property of the outcropping surface ocean. The LS mode had higher atmospheric pCO_2 because the deep ocean outcroped through the warm, low latitude surface ocean which was poor in DIC concentration.

Chapter 3 compared the fully-coupled and the semi-coupled AOC models and showed that the C system had weak feedbacks on the AO system, and that the first-order system behavior of the AOC system was determined by the AO system.

Chapter 4 described four important feedback mechanisms in the AOC system with the Clausius-Clapeyron relationship. Figure 4-5 explained the global warming feedback and the thermohaline pCO_2 feedback in the electric circuit type of representation. The outgassing feedback and the biological pump feedback tends to cancel out each other in the AOC model. Chapter 4 also simulated an idealized global warming where an external source rapidly raised the atmospheric pCO_2. Numerical experiments showed that the feedback mechanisms had significant effect on the rate of increase in pCO_2. The four feedback mechanisms imposed a net positive feedback in the idealized global warming simulation.

5.2 Comparison with previous studies

Figure 1-2 shows that pCO_2 was tightly correlated with the temperature of the air near the polar region (23) for the last 50,000 years. When the air is warmer, it has higher atmospheric pCO_2, and when the air is cooler, it has lower atmospheric pCO_2. In this study, the global warming feedback related the global mean temperature and the atmospheric CO_2. Positive anomaly in the temperature causes a decrease in solubility of gases in water. It reduces the capacity of the ocean for CO_2, therefore it increases atmospheric pCO_2. The increased pCO_2 further enhances the original positive anomaly in the temperature. This argument is consistent with the Figure 1-2. The global warming feedback could represent a possible mechanism of the tight coupling between the atmospheric pCO_2 and the temperature in the ice core records.

Sarmiento and Quere suggested that the collapse of the thermohaline circulation can cause the considerable reduction of the CO_2 uptake by the ocean (25). Their numerical experiment was based on an ocean-atmosphere coupled general circulation model (GCM) with several different assumptions on the oceanic ecosystem. The model without the biological processes showed that a gradually increasing pCO_2 could cause a large reduction in the oceanic CO_2 uptake because of the increased sea surface temperature and the halt of the thermohaline circulation.

In this study, the global warming heats up the ocean, and it then increases the

atmospheric pCO_2 through the global warming feedback. The DIC exporting feedback could also explain the reduction of the CO_2 uptake in the GCM experiment. Global warming tends to weaken the thermohaline circulation through the Clausius-Clapeyron relationship. The weakening of the thermohaline circulation makes the vertical DIC transport inefficient between the high latitude surface ocean and the deep ocean. Therefore, the weakening of the thermohaline circulation could reduce the oceanic CO_2 uptake through the DIC export feedback.

When the biological model is not coupled with the thermohaline circulation, the weakening of the thermohaline circulation does not affect the particulate flux. The AOC model can set the particulate flux independent of the thermohaline intensity by fixing the surface nutrients concentration. However, in the coupled AOC system, the weakening of the thermohaline circulation decreases the surface nutrients concentration and it could results in a reduction in the particulate flux. Therefore, the biological pump feedback and the outgassing feedback tends to cancel out each other in the coupled AOC system. The constant Biota model could overestimate the oceanic CO_2 uptake.

5.3 Possibilities for future expansion

This study is an attempt to understand several fundamental mechanisms of the interactions in the atmosphere-ocean-carbon system. Chapter 2 introduced a new parameterization of the carbon chemistry which made it possible to understand the effect of SST and SSS in a transparent way. The parameterization treated the alkalinity in two different ways. First, it assumed total alkalinity as constant everywhere. Second, it treated the alkalinity as a linear function of SSS, which implies that the model treats alkalinity and the salinity in a similar way. The model was very sensitive to the assumption on alkalinity. Alkalinity is affected by the advective transport, evaporation and precipitation, and the biological activity. Therefore, there is a need to add an alkalinity cycle model to the AOC system to obtain more realistic representation for the carbon chemistry.

Manabe and Stouffer (18), and Stocker and Schmittner (28) showed that the anthropogenic global warming could halt the thermohaline circulation in their GCM study. In this study, the AOC model only allows the high latitude sinking (HS) mode and the low latitude sinking (LS) mode. The halt of thermohaline circulation does not mean that the system attains the LS mode in the GCM experiments. Shutdown of the thermohaline circulation in the GCM experiments is a complicated issue and is fundamentally different from the transition from the HS mode to the LS mode in the idealized AOC model. It is necessary to include some representation for the interhemispheric flow and the geometry of the ocean which is closer to the current ocean, if one is to simulate the halt of the thermohaline circulation due to the anthropogenic global warming.

Bibliography

1. J. Ahmad, G.B. Paklar, F. Bonjean, G.D. Bo, T. Kaminski, F. Kauker, M. Monai, E. Pierazzo, P. Stone, and L. Zampato, (1997), The interaction between global warming and the thermohaline circulation, Environmental Dynamics Series.V: Hydrometeorology and Climatology, Istituto Veneto di Scienze, Lettere ed Arti, Venice, Edited by M. Marani and R. Rigon, pp.87-100

2. R.B. Bacastow, (1993), The effect of temperature change of the warm surface waters of the oceans on atmospheric CO2, Global Biogeochemical Cycles, 10(2), pp.319-333

3. B. Bolin and E. Eriksson, (1959), Changes in the carbon dioxide content of the atmosphere and sea due to fossil fuel combustion, Distribution of matter in the sea and atmosphere, Edited by B. Bolin, International Meteorological Institute in Stockholm, New York, pp.130-142

4. P.G. Brewer, A.L. Bradshaw and R.T. Williams,(1986), Measurements of total carbon dioxide and alkalinity in the Northern Atlantic Ocean in 1981, The changing carbon cycle : A global analysis, Edited by J.R. Trabalka and D.E. Reichle, Springer-Verag, New York, pp.348-370

5. W.S. Broecker, D.M. Peteet and D. Rind, (1985), Does the ocean-atmosphere system have more than one stable mode of operation ?, Nature, 315, pp.21-26

6. W.S. Broecker and G.H. Denton, (1989), The role of ocean reorganization in glacial cycles, Geochemica et Cosmochimica Acta, 53(10), pp.2465-2501

7. W.S. Broecker and T.H. Peny, (1993), Greenhouse puzzles, Eldigio Press, Lamont-Dohery Observatory of Columbia University

8. F. Bryan, (1986), High-latitude salinity effects and interhemispheric thermohaline circulation, Nature, 323, pp.301-304

9. W. Dansgaard et al, (1982), New Greenland deep ice core, Science, 218, pp.1273-1277

10. E. Eriksson, (1963), Possible fluctuations in atmospheric carbon dioxide due to changes in the properties of the sea, Journal of Geophysical Research, 68(13), pp.3871-3876

11. M.J. Follows, R.G. Williams, and J.C. Marshall, (1996), The solubility pump in the subtropical gyre of the North Atlantic, Journal of Marine Research, 54(4), pp.605-630

12. C. Goyet and A. Poisson, (1989), New determination of carbonic acid dissociation constants in seawater as a function of temperature and salinity, Deep Sea Research, 36(11), pp.1635-1654

13. M.M. Hall and H.L. Bryden, (1982), Direct estimates and mechanisms of ocean heat transport, Deep Sea Research, 29, pp.339-359

14. J. Hansen, I. Fung, A. Lacis, D. Rind, S. Lebedeff, R. Ruedy, G. Russel and P.H. Stone, (1988), Global climate changes as forecast by Goddard Institute for Space Studies three dimensional model, Journal of Geophysical Research, 93(D8), pp.9341-9364

15. F. Joos, G. Platter, T.F. Stocker, O. Marchal, and A. Schmittner, (1999), Global warming and marine carbon cycle feedbacks on future atmospheric CO2, Science, 284, pp.464-467

16. F. Knox and M. McEloy, (1984), Changes in atmospheric CO2 : Influence of biota at high latitudes, Journal of Geophysical Research, 89, pp.4629-4637

17. A.M. Macdonald and C. Wunsch, (1993), An estimate of global ocean circulation and heat fluxes, Nature, 382, pp.436-439

18. S. Manabe and R.J. Stouffer, (1993), Century-scale effects of increased atmospheric CO2 on the ocean-atmosphere system, Nature, 364, pp.215-218

19. J. Marotzke and J. Willebrand, (1991), Multiple equilibria of the global thermohaline circulation, Journal of physical oceanography, 21, pp.1372-1385

20. J. Marotzke and P.H. Stone, (1995), Atmospheric transports, the thermohaline circulation, and flux adjustments in a simple coupled model, Journal of Physical Oceanography, 25, pp.1350-1364

21. J. Marotzke, (1996), Analysis of thermohaline feedbacks in Decadal Climate Variability, Dynamics and Predictability, I 44, NATO ASI, Edited by D.L.T. Anderson and J. Willebrand, Springer-Verlag, Beriln Heidenberg, pp.334-378

22. V. Ramanathan, M.S. Lian and R.D. Cess, (1979), Increased atmospheric CO2 : zonal and seasonal estimates of the effect on the radiation energy balance and surface temperature, Journal of Geophysical Research, 84, pp.4949-4958

23. D. Raynaud et al, (1993), The ice record of greenhouse gases, Science, 259, pp.926-934

24. J.L. Sarmiento and J.R. Toggweiler, (1984), A new model for the role of the oceans in determining atmospheric pCO2, Nature, 308, pp.621-626

25. J.L. Sarmiento and C.L. Quere, (1996), Oceanic carbon dioxide uptake in a model of century-scale global warming, Science, 274, pp.1346-1350

26. J.L. Sarmiento, T.M.C. Hughes, R.J. Stouffer and S. Manabe, (1998), Simulated response of the ocean carbon cycle to anthropogenic climate warming, Nature, 393, pp.245-249

27. U. Siegenthaler and J.L. Sarmiento, (1993), Atmospheric carbon dioxide and the ocean, Nature, 365, pp.119-125

28. T.F. Stocker and A. Schmittner, (1997), Influence of CO2 emission rates on the stability of the thermohaline circulation, Nature, 388, pp.862-865

29. J.C.G. Walker and J.F. Kasting, (1992), Effects of fuel and forest conservation on future levels of atmospheric carbon dioxide, Palaeogeography, Palaeoclimatology, Palaeoecology (Global and planetary change section, 97, pp.151-189

30. R.F. Weiss, (1974), Carbon dioxide in water and sea water : the solubility of a non-ideal gas, Marine Chemistry, 2, pp.203-215

31. T. Wenk and U. Siegenthaler, (1985), Natural variations Archean to Present, AGU, Washington DC.